Atomic scale modification of semiconductor nanostructure surfaces

B. Sc. thesis of 15 credits

by Robin S† Svärd
robinsward@telia.com

Supervisors: Prof. Anders Mikkelsen
PhD student Johan Knutsson

Abstract

The III-V semiconducting compounds InAs and GaSb were studied using scanning tunneling microscopy (STM) and X-ray photoelectron spectroscopy (XPS). Different crystal planes of each material were investigated separately, including wafers of InAs(111)A, InAs(111)B, InAs(110), GaSb(100), GaSb(110) as well as nanowires consisting of InAs. All these materials were imaged both before and after exposure to atomic hydrogen along with moderate annealing in order to compare and characterize changes of the surface morphology. Generally, a high success rate for cleaning with atomic hydrogen was established, with atomic resolution achieved for InAs(111)A, InAs(110), GaSb(100) and the nanowires. Conclusions regarding reconstructions of the surfaces were made from STM measurements, and regarding remnant oxides and the efficiency of the cleaning recipes from XPS data.

Robin S. Svärd

Ytfysik – Hur man ser utan att se

Vad är egentligen en yta? Beroende på sammanhang kan nämligen själva definitionen av vad en yta är variera, och under en väldigt lång tid har det optiska mikroskopet använts som en förlängning av det mänskliga ögat. Men det finns en gräns på hur djupt synligt ljus kan nå, och detta är tyvärr inte djupt nog för att se den *faktiska* ytan hos ett material. Man ska dock inte glömma att även blinda kan se... åtminstone i viss mening; nämligen genom att känna. Det är denna grundtanke som ligger bakom det Nobelprisbelönta *sveptunnelmikroskopet* (STM).

Instrumentet bygger på att en extremt vass spets – där själva toppen består av en enda atom – förs väldigt nära ett material utan att någonsin röra vid det. Genom att lägga på en spänning så kommer elektroner att börja röra sig mellan spetsen och ytan. Denna lilla ström av elektroner går att mäta, och genom att föra omkring spetsen på ytan så kan den avbildas till en digital bild. På så sätt kommer man alltså "se" hur ytan ser ut, enbart genom att känna på den. Upplösningen på dessa bilder kan dessutom bli tillräckligt hög att särskilja enstaka atomer på ytan!

En stor del av vetenskapen drivs just nu för att miniatyrisera komponenter, vilket oundvikligen leder till att allt fler interaktioner tar plats på ytan. Just ytatomerna är dessutom av extra stort intresse då deras kemiska och fysiska egenskaper ofta skiljer sig drastiskt från resten av atomerna inuti materialet. Det är därför av särskilt stor betydelse att man på en atomär skala vet hur ytan ser ut för att kunna dra slutsatser om materialets egenskaper. Problemet är ofta att *alla* ytor är mer eller mindre smutsiga och måste först rengöras.

Vi har studerat de två halvledande föreningarna *indiumarsenid* (InAs) och *gallium antimonide* (GaSb) främst m.h.a. ett STM. Dessa har rengjorts genom exponering till atomärt väte som binder sig till föroreningarna på ytan och tar dem med sig vid upphettning. Ett flertal olika kristallplan av varje material undersöktes både före och efter exponering till vätet i ett försök att kartlägga förändringar på ytan.

Generellt uppnåddes goda resultat för rengöring med atomärt väte, och atomär upplösning erhölls för InAs(111)A, InAs(110) och GaSb(110). Ytterligare slutsatser angående rekonstruktion av ytatomerna kunde dras från bilderna. Den huvudsakliga anledningen till varför just dessa två material undersöktes är för framtida planer att utveckla komponenter bestående utav båda för en mängd olika ändamål. Det är därför nödvändigt att kunna rengöra båda material samtidigt under omständigheter som inte förstör någon utav dem.

Contents

1 Introduction and Motivation

What is this thing called surface science?

Long story short, the field of surface science involves exploring the chemical and physical interactions between any interface of a solid — such as the surface — and its surroundings. Not too long ago, scientists were restricted to e.g. electrical or optical measurements after preparing a sample, thus limiting the amount of information which could possibly be obtained from a given material. In the early 1980s, the entire field of surface science was revolutionized with the invention of the *scanning tunneling microscope* (STM). No longer restricted to the whole concept of *"cook and look"*, it is now possible to probe at an atomic level how the sample changes and how this change can contribute to why new traits arise. This makes the entire field of surface science rather young, with a history dating back barely 50 years.

Much of the strong interest in nanotechnology originates from the fact that many materials drastically change their properties at a small enough scale; properties which will dominate the entire nano-object given that the structure is sufficiently small. Technology of the 21st century appears completely driven by a desire to miniaturize every complex device possible, which inevitably leads to the surfaces of said devices being of exceptional importance for characterizing their functions and properties. This significance is even further increased when dealing with 1D nanostructures such as nanowires, where the actual surface-to-bulk ratio starts to reach critical values and even more interactions takes place at the surface.

Roughly speaking, some scientists who grow nanowires only see, which to them, wires which looks perfectly healthy. Engineers build devices of out said wires and will only see the electrical measurements which is later used to e.g. define the efficiency of a solar cell. This is where the field of surface science comes in; with the tools available to probe the very atomic structure of the nanodevices. This way, is it possible to see, among many other things, the actual junction between the P and N doped regions of a semiconducting structure or possible flaws and faults caused during nanowire growth. This information will then be very relevant to future growth of nanowires and how to handle the devices made out of them.

Although, everything does not have to revolve around the manufacturing of structures, but sometimes, one must instead *remove* things in order to awaken new properties in materials. The primary theme of the present work is a series of different processes which all, in one way or another, remove something from the material in question. The treated materials are subsequently investigated using various tools and methods in order to find and explain what actually happened.

Surfaces of any material are generally littered with native oxides and other contaminations as a result of exposure to open air, hiding in plain sight even to the sharpest optical microscope, and these will often shroud the true characteristics of a material. Hence, it is of utmost importance that the actual surface is atomically clean and rid of contaminations before any delicate devices are built out of them. However, in order to check if e.g. nanowires are successfully cleaned, a lot of time and effort can be saved by first making sure that entire wafers of the same material as the nanowires can be cleaned using the present methods, as they typically exhibit similar properties.

The work presented in this thesis will primarily be centred around the III-IV semiconducting compounds *Indium Arsenide* (InAs) and *Gallium Antimonide* (GaSb). These two specific materials were investigated due to a long term goal being the construction of devices containing nanowires consisting of *both* InAs and GaSb. A primary aim of this thesis have been to attempt to find a cleaning recipe which works for both InAs and GaSb under temperatures which would not ruin either of the materials.

Everyday I'm tunnelin', tunnelin'...

2 The Actual Surfaces of Materials

The everyday interactions between any kind of solid and its immediate surroundings takes place at the *surface* of the material. However, the empirical definition of a surface on a macroscopic scale is often vastly different than that on the atomic scale.

It is down at the individual atoms that the actual interaction takes place, much like when sitting in a chair one is actually *suspended* in the air due to the repelling nature of the electrons. We do not simply merge and become one with everything we touch, otherwise there wouldn't be any horror science-fiction. When dealing with the atomic scale, the surface is often defined as the region where the properties of the atoms differ from the bulk atoms in any way, such as their atomic bonds.

In order to properly investigate and characterize the surfaces of materials, some general understanding of crystalline structures is required and will be given in the following sections, focusing on the areas of particular relevance to this thesis.

2.1 Surface Structures and the Crystal Lattice

In general, only an extremely limited amount of atoms make up the surface of a given solid in comparison to its bulk. Even for a single grain with a size in the order of 1000^3 atomic distances, its boundary will only consist of about 0.1% of the total atoms, the rest being locked in a perfectly crystalline environment [1]. Further, the interesting thing about this environment is that the atomic arrangement within the bulk are (more or less) completely defined by a periodic translation of a single, often rather simple three-dimensional element known as the *unit cell*. Due to the fact that most solids exhibit a crystalline structure, one can argue that the surface of the material is wherever the lattice symmetry of the unit cell is broken.

Since the bulk of a solid can be expressed as a spatially repeated structure, it seems only reasonable to describe this periodicity in terms of its simplest, namely its *fundamental unit cell*, possessing the smallest volume of all possible unit cells describing the material. Henceforth, the fundamental unit cell will simply be referred to as the unit cell. For most materials, a simple cubic unit cell, illustrated in fig. 1(a), is an important starting point even though the structure itself is not very common. The dimension of the unit cell is based on the translational and orthogonal base vectors $\mathbf{a}_1$, $\mathbf{a}_2$ and $\mathbf{a}_3$, which together define the direction of a lattice plane which intersects the x-, y- and z-axis, respectively. This in

turn also defines the *lattice constant a* as the distance between two adjacent lattice points. Depending on how the base vectors are oriented, several lattice configurations are possible while all such possible configurations are collectively referred to as *Bravais lattices*.

However, the atoms in metals do not have any preferences regarding directional bonding and the atoms therefore prefer more close-packed structures than the simple cubic structure. The packing density is immediately improved in the *body-centred cubic* (bcc) and the *face-centred cubic* structures (fcc), as illustrated in fig. 1(b) and fig. 1(c), respectively.
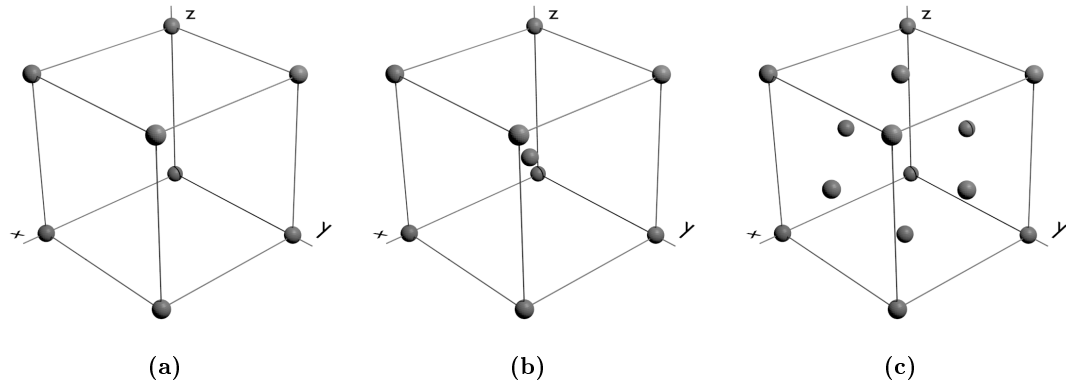

(a)   (b)   (c)

Figure 1: The three different cubic Bravais lattices. The *simple cubic* unit cell is shown in (a), consisting of one lattice point (or atom) in each corner of the cube. It is therefore said that the unit cell contains 1 atom in total, as each atom is shared equally between eight adjacent unit cells. The bcc shown in (b) contains an additional lattice point in the center of the cube, and thus contains a total of 2 atoms, while the fcc shown in (c) has lattice points on each of the faces of the cube, resulting in a total of 4 atoms per unit cell.

The lattice planes defined by the three vectors $\mathbf{a}_1$, $\mathbf{a}_2$ and $\mathbf{a}_3$ may just as well be characterized by a set of three integers known as *Miller indices*, typically denoted as (*hkl*). These Miller indices will basically represent the integer inverse values of the translational base vectors. Both the structure of the surface and its orientation will be directly dependant on how the unit cell is cut by the lattice plane, which is illustrated in fig. 2(a−c). A specific structure can be obtained by e.g. mechanical cutting of the material or even during its manufacturing, as will be discussed in later chapters regarding nanowires.

Additionally, a very fundamental and essential part of crystal structures will be left out of this thesis, namely the *reciprocal space lattice*, since nothing of the sort was encountered during the present work. Represented as the *Fourier transform* of the real-space lattice, the reciprocal space acts as the very foundation for certain experimental methods such as *low-energy electron diffraction* (LEED) and it is typically explained in detail in any introductory literature regarding solid state physics.
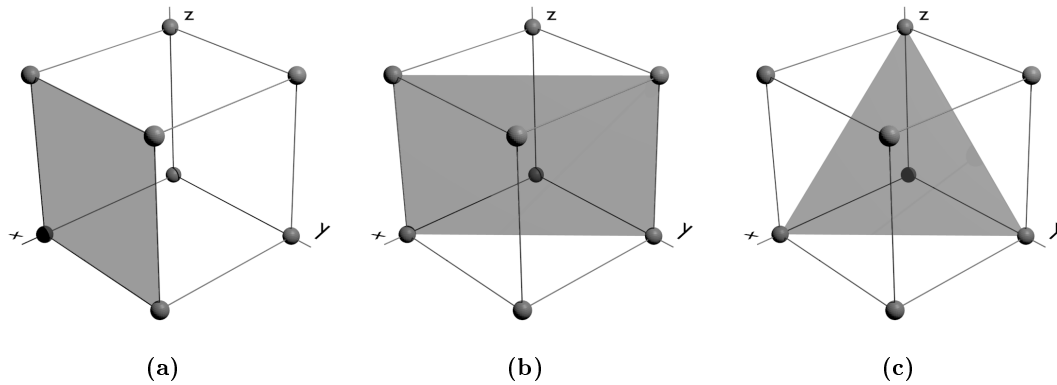
(a)   (b)   (c)

Figure 2: Miller indices, or (hkl), is a convenient and straightfor-
ward way of noting different planes in Bravais lattices. For example,
the plane represented in (a) is denoted as (100), being the integer in-
verse values of the vectors (a, ∞, ∞). In the same manner, (b) shows
the plane (110) while (c) shows the plane (111).

When it comes to the actual stacking of the lattice planes defined by the *Miller indices*,
there are generally two ways, as aptly illustrated in fig. 3(a) and fig. 3(b). These are
known as *face-center cubic* (FCC) stacking and *hexagonally close packed* (HCP) stacking,
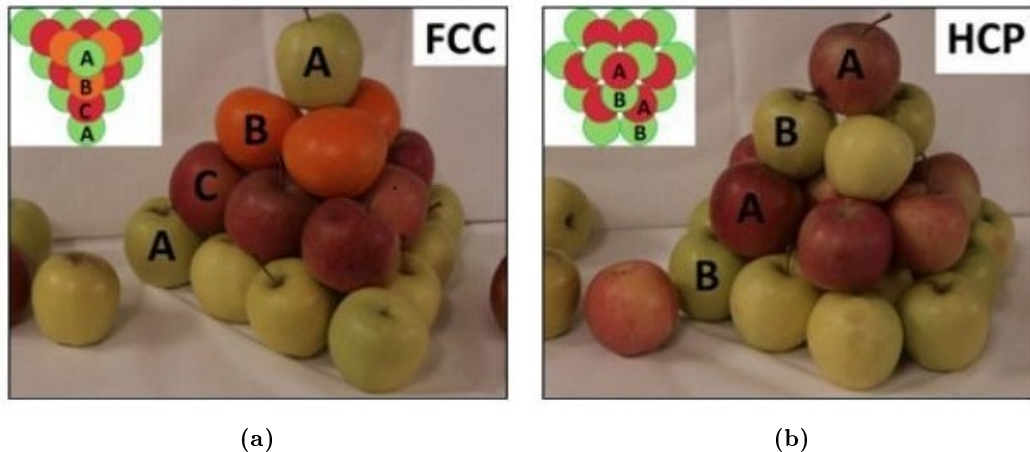respectively.

(a)   (b)

Figure 3: FCC stacking is shown in (a) using a triangle shape as
a base, arranged such that each layer is periodically repeated every
three layers of the structure. Similarly, HCP stacking is shown in
(b) using a hexagonal shape as a base, arranged such that each layer
is repeated every two layers instead. This implies that there exist a
"natural" desire for closely packed structures; not only when stacking
apples in order to obtain maximum packing density, but just as well
on an atomic scale. Images from ref. **[2]**.

2.1.1   Relaxation, Reconstruction and Adsorption

Whenever a surface of a crystal is formed in any way, the sudden symmetry breaking of the otherwise periodic atomic structure will cause significant stress to the sub-surface crystal layers. This will result in the surface atoms attempting to minimize the surface energy, and there are a few different ways to achieve this with the two most common being *relaxation* and *reconstruction*.

Both relaxation and reconstruction will relieve the stress on the surface by re-arranging the surface potential. When dealing with metals, the former will alter the interatomic distance by decreasing the distance between atomic layers which lies parallel to the surface, although this phenomena was not extensively encountered during the present work. If the bulk crystal lattice remain preserved when the surface is formed, a reconstruction might occur instead. While in the bulk, each atom is surrounded by a set of neighbouring atoms, satisfying all the atomic bonds. However, when a surface is formed, any atom exposed at the boundary will have unsatisfied atomic bonds due to the reduced degrees of freedom, resulting in the surface atoms re-arranging in order to satisfy any energetically unfavourable dangling bonds which might have been produced when the surface was formed. If the general structure of the surface differs from that of the bulk, then the surface is considered reconstructed. This, in addition to relaxation, are illustrated in fig. 4(a) and fig. 4(b), respectively.

Depending on the surroundings during surface formation, a third option to minimize the surface energy is also plausible, namely *adsorption*. Due to the abrupt potential change at the surface, local potential "peaks" or "dips" might form and with dangling bonds present, the surface might then adsorb adatoms from its immediate vicinity. This is illustrated in fig. 4(c). Adsorption of adatoms and native oxides is very common and unfortunately poses a great hinder for almost any kind of study of the surface, as will be discussed in later sections.
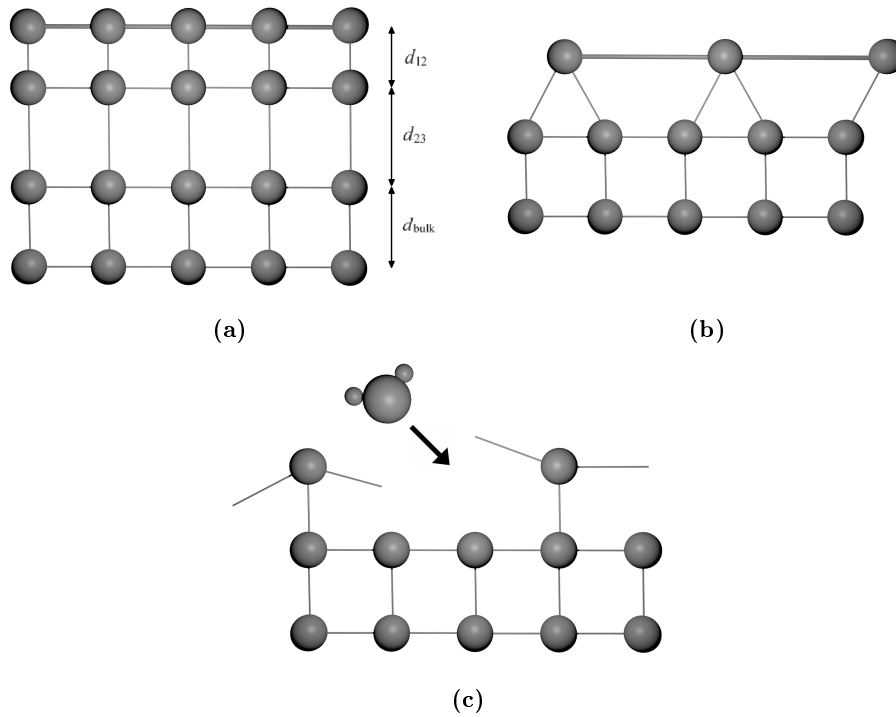
(a)   (b)

(c)

Figure 4: The three most common ways for the materials to relieve stress on the surface. *Relaxation* is shown in (a), where the actual atomic structure remains the same although the distances between the near-surface layers, d_{12} and d_{23}, has been shifted relative to the bulk distances d_{bulk}. *Reconstruction* is shown in (b), where dangling bonds on the surface atoms can be satisfied by rearranging the top-most layer, thus breaking the periodicity of the bulk atoms. The event of *adsorption* is illustrated in (c), where an adatom may end up getting caught in the dangling bonds present at the surface.

2.2 Some Nanowires Characteristics

As the dimensions of a nanostructure is further reduced, the surface-to-volume ratio is increased and at some critical value, various properties of the nanostructure such as electrical or optical will be dominated by its surface rather than its bulk. As is the case with nanowires; the morphology of the nanowire facets are of exceptional importance, and must thus be fully understood before proper devices can be manufactured out of said wires.

Because of the many interesting features that nanowires exhibit caused by the high surface-to-volume ratio, they are considered by many as the path to future technology. Much like the bulk of any other material, the sub-surface layers of nanowires should behave just the same. Although the actual art of growing nanowires has been described in detail elsewhere [3], its worth mentioning that they are generally grown with high precision as freestanding rods whose dimensions can be specifically tailored for various purposes, with a diameter measured in tens of nanometers and a length of up to several micrometers. The various facets of the nanowires can be further tailored depending on what substrate the wires are grown on, opening up for even more possibilities.

Additionally, nanowires show crystal formations rarely found anywhere else; namely the hexagonal Wurtzite (WZ) structure which was briefly studied during the present work. As typical *transmission electron microscopy* (TEM) studies only reveal the general structure and stacking faults obtained during growth, the application of even more precise instruments is necessary in order to map out the actual morphology of the nanowires, as will be described in the next section.
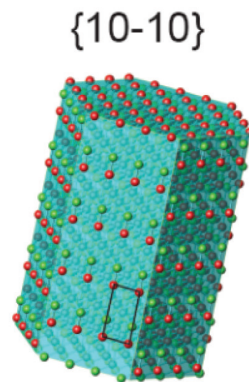

Figure 5: 3D model of the hexagonal Wurtzite structure with one of the most common crystal facets when grown on a (111)B substrate, namely $\{10\bar{1}0\}$. Image taken from ref. [4]

3   A Brief History of Instrumental Techniques

Throughout the thesis, several experimental tools and methods were used in the investigation of the various surfaces. However, undoubtedly the most important ones were the *scanning tunneling microscopy* (STM) followed by *X-ray photoelectron spectroscopy* (XPS), both described in detail in this chapter.

3.1   Scanning Tunneling Microscopy (STM)

The world of quantum mechanics is a fascinating, yet sometimes rather strange in comparison to our macroscopic world. At the atomic scale where wavefunctions are used to describe interactions between matter, one of the many possible occurrences is that of *quantum tunneling*. First presented in the early 1980s by Gerd Binnig and Heinrich Rohrer [5, 6], the discovery that electrons could tunnel between two conducting surfaces through vacuum quickly led to the invention of the *scanning tunneling microscope*, later resulting in the group being awarded the Nobel prize in physics in 1986. This new method of controlling the structure of conducting sample surfaces with atomic precision in real space revolutionized the way the surfaces of materials were treated, allowing for a vast amount of new discoveries. [7, 8] Since then, STM measurements can almost be considered a necessary complement in the manufacturing of modern electronic devices.

The very backbone of the STM is in theory rather simple: an atomically sharp tip − meaning that the actual apex of the tip can be approximated to a single atom − is brought sufficiently close to the sample surface to allow electrons to propagate through the vacuum barrier in between the sample and the tip, creating an electrical tunneling contact. However, as the Fermi levels of the sample and the tip are aligned while in electrical contact, no net current will flow as illustrated in fig. 6(a).

In order for a detectable current to flow from one material to another, a bias or gap voltage V_g must be applied to the sample, allowing a tunneling current I_t to flow, typically in the order of pA-nA. Further, the sign of the gap voltage will determine the direction of the tunneling current. A positive bias will allow electrons to tunnel from the tip to the sample, thus probing empty electron states on the surface, while in a negative bias electrons will tunnel from the sample to the tip, probing filled electron states. These two modes are

illustrated in fig. 6(b) and fig. 6(c), respectively. While certain polyatomic materials exhibit different topographic structure depending on the sign of the gap voltage, nothing of the sort was encountered during the present work. It is also worth mentioning that when scanning on semiconducting samples, an applied bias greater than the band gap of the material is essential. The tip would otherwise attempt to probe the at the Fermi level void of empty states for the electrons to tunnel to, thus resulting in the tip crashing into the sample as there would be no feedback loop to stop it.
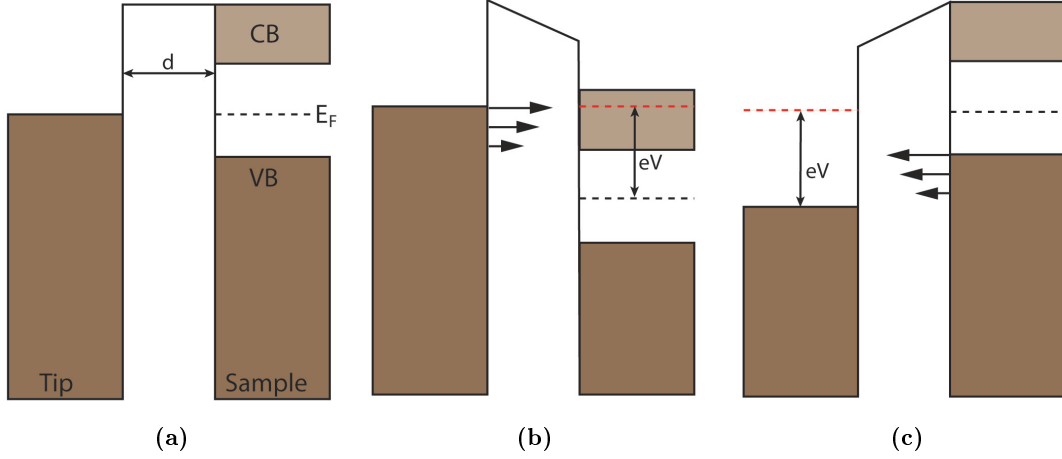

(a)   (b)   (c)

Figure 6: Representation of the Fermi levels in order to illustrate how the tunneling current depends on the polarity of the applied sample bias. In (a), the tip and sample are in electrical contact and no net current will flow. In (b), a positive bias is applied, resulting in electrons tunneling from the tip to empty electron states in the conduction band (CB). Likewise, when a negative bias is applied, electrons will tunnel from the valence band (VB) to the tip, as seen in (c). Image from ref. **[9]**.

G.Binnig and H. Rohrer proposed that the tunneling current I_t can be estimated by **[10]**:

$$I_t \propto (V_g/s) \exp(-A\Phi^{1/2}s) \tag{1}$$

where V_g is the applied voltage bias and $A = 1.025$ eV$^{-1/2}$ Å^{-1} for a vacuum barrier. The average work function Φ is assumed equal to the mean barrier height between the tip and the sample, and s is the tip-sample separation, typically in the region of 10 Å. In order for keeping V_g and I_t constant (provided Φ remains constant as well), only the tip-sample separation s should be varied. This will result in the surface topography being recorded while scanning.

Due to the exponential relation, the magnitude of the tunneling current is almost solely defined by the actual distance between the tip and the sample, resulting in a very high lateral resolution of the images. Additionally, it also follows from this exponential relation that the vertical resolution will be very high, thus ensuring that only the atom closest to the tip will be imaged.

There are generally two ways to operate an STM. In the first mode, dubbed the *constant-current* mode (CC), the tunneling current is maintained at a pre-set value using an active feedback loop while scanning. In doing so, the trajectory of the tip apex will map out a profile of the sample topography by controlling the tip-sample separation, approaching or retracting the tip depending on changes on the surface. The vertical displacement of the tip as a function of sample position can thus be translated into an image of the surface. This mode is illustrated in fig. 7. While the constant-current mode is arguably the most widely used, the second operating mode of an STM relies on scanning the sample surface at a constant height, thus measuring the variations in the tunneling current instead with the feedback loop turned off. This mode is called *constant-height* mode (CH). While it is possible to scan at a faster pace and it should, in theory, yield just as detailed images as the constant-current mode, the risk of crushing the tip into a sudden elevation of the sample surface is very high unless it is intrinsically very flat. Hence, this mode was not used during the work presented in this thesis.
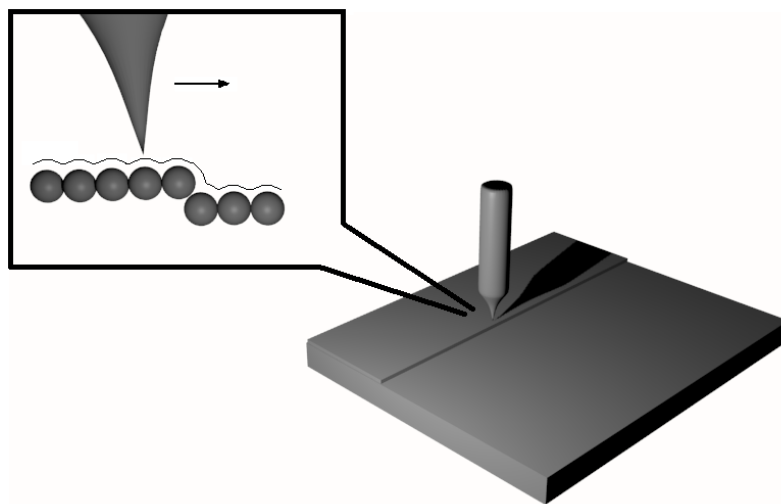

Figure 7: Illustration of an STM running in a *constant-current mode*. In this mode, the apex of the tip will retract and approach depending on the surface morphology. The resulting image will thus include distinct features such as steps and terraces and, given optimal circumstances, the individual atoms themselves.

The actual movement of the tip is achieved using piezoelectric elements, capable of next-to instantaneous displacement with very high precision. However, the factor regarding the exponential relation still plays a crucial role and the tunneling current is thus extremely sensitive to changes in the sample morphology, even if these changes can be accounted for very quickly. Because of this, atomic resolution is generally very hard to achieve unless the sample surface is sufficiently flat already.

It is also worth mentioning that a powerful tool often used in connection with STM imaging is the *scanning tunneling spectroscopy* (STS), capable of locally probing the electronic properties around the Fermi level of a material even during scanning. This information can then be used for various purposes, including tweaking of the applied gap voltage in an attempt to obtain better spatial resolution of the STM images. However, STS was only sparsely used during the present work and will not be discussed further.

In summary, STM will yield highly resolved images of real space surfaces using a non-destructive investigative method.

3.1.1 STM Image Interpretation

When imaging on a large enough scale, that is in the range of tens to a few hundreds nanometer, STM images will under optimal circumstances provide very reliable information regarding the topography of the sample, including features such as terraces, atomic steps, oxides etc. However, one of the major downsides of STM imaging is the fact that the surface itself is never *observed directly*, but only the local electron density of states at the surface. It is thus possible for various artifacts to emerge in the images, and a fair amount of thoughtfulness is necessary when attempting to interpret this data. These artifacts might originate from several different sources, although the most probable one is from the tip itself.

Ideally, all the theory regarding STM measurements predict a symmetrical tip with an apex consisting of a single atom. In reality, this is not always the case, and the quality of the resulting image is greatly influenced by the condition of the tip. The STM images may hint on a damaged tip in various ways, including instabilities and features appearing larger with distorted shapes. Another occurrence, which unfortunately is very common, is that the tip will pick up adatoms from the sample surface due to the applied bias. Picking up and later dropping these adatoms will typically register as sudden spikes in the measured current, causing the tip to retract rapidly. However, as this effect will be confined to a single scan-line, it can be retrospectively accounted for by either excluding the data altogether or averaging it using the neighboring lines, as they are an inherit defect of the experimental method. Extra persistent adatoms can be manually deposited onto the sample surface by running a quick voltage pulse of up to 10 V through the tip for approximately 1 ms.

Additionally, "*multiple tips*" may also form, resulting in features being repeated due to the final image being a convolution between all the images from all the tips. A theoretical scenario as well as a real-space image of a double-tip can be seen in fig. 8(a) and 8(b), respectively.
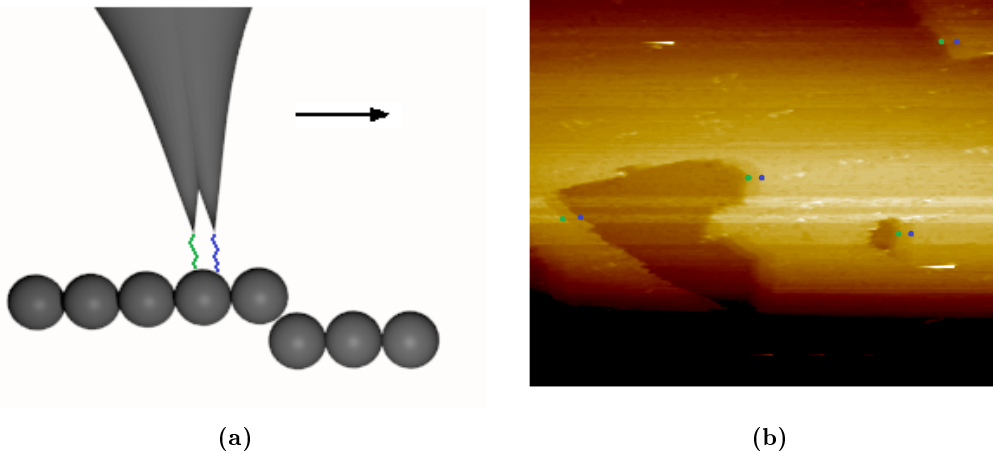

(a)   (b)

Figure 8: In (a), a theoretical interpretation of a double-tip is illustrated, where the second tip (green) will image everything slightly after the first tip (blue). This will cause all distinct features to appear twice, as can be seen in (b). The distance between the mirrored features will thus correspond to the actual real-space distance between the two tips.

Further artifacts which might emerge in the STM images are that of thermal drift or creep caused by ghost-currents in the piezoelectric elements [11], present as a remnant from coarse movements such as approaching the sample. Both of these will cause the resulting image to appear distorted and smeared out just as if the substrate itself was moving. Nevertheless, this can easily be avoided with some patience, by allowing the sample to cool down properly or the piezoelectric elements to relax for a moment. These two phenomena are presented in fig. 9(a) and fig. 9(b), respectively.

Proper prevention of vibrations is also essential for STM measurements and something which will be discussed in later sections regarding the STM used during the present work.
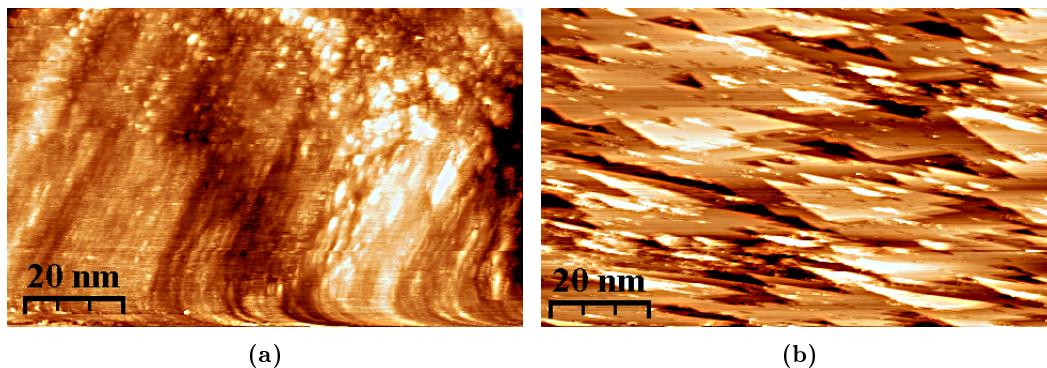
(a)   (b)

Figure 9: Drift caused by coarse movements with the piezoelectric elements can be seen in (a), where the bottom of the image appears distorted just as if the sample surface was moving. Worth noticing is that the ghost-currents must first dissipate completely before any of the lumpy features could be observed. Likewise, thermal drift can be seen in (b), where the entire image appears flattened caused by imaging the sample too quickly after it had been heated.

3.2   Synchrotron Radiation and XPS

There are yet further ways to probe the surfaces of materials, one of them being based on the effect of *light-matter interaction* first presented by Heinrich Hertz in 1887 [12], which later led Albert Einstein in 1905 to formulate his explanation of why only photons of certain energy were capable of knocking electrons out of matter. This phenomenon, now generally known as the *photoelectric effect*, resulted in Einstein being awarded with the Nobel prize in physics in 1921 and is usually described by:

$$E_{kin} = \hbar\omega - E_B - \phi \tag{2}$$

where E_{kin} is the kinetic energy of the emitted electron, $\hbar$ is Planck's constant, ω is the radiation frequency of the incident photon, E_B is the binding energy of the electron and ϕ is the work function relating the vacuum level to the Fermi level of the solid. In order for the photoelectric effect to occur, the incident photon must have an energy $\hbar\omega$ that is higher than the binding energy of the electron orbit it is meant to probe, the excess photon energy being used to define E_{kin}.

Since the binding energies of the electrons are element specific, monochromatic radiation of known energy can be used to determine a relation between the kinetic energies of the emitted electrons, henceforth referred to as *photoelectrons*, and their corresponding binding energies. This way, it is possible not only to find fingerprints of a particular element in a sample, but also distinguish between different chemical states of the element, resulting in photoelectron spectroscopy being an incredibly useful tool in many research areas.

X-ray photoelectron spectroscopy (XPS), as the name implies, corresponds to a certain energy range of excitation radiation with photon energies of 150-2000 eV. This specific energy range is exceptionally interesting, as the core level binding energies of every element with an atomic number greater than 3 (lithium) fit into this range. In order to properly evaluate the presence of a specific element in the sample, its photoelectron spectrum can be completely decomposed into its different chemical states individually, with their intensities proportional to the number of atoms in each chemical state.

The kinetic energy of the photoelectrons, E_{kin}, is measured by an hemispherical electron analyzer (HSA), consisting of two concentric hemispheres of different potential. The details have been explained elsewhere [13], but the basic idea is that only photoelectrons of a specific kinetic energy will reach the analyzer, the rest hitting the conducting hemispheres due to either being too fast or too slow and thus get picked up by the electric field between the plates.

For these types of experiments, a continuous, monochromatic and coherent radiation source of adjustable photon energy is highly desirable, and for this purpose, entire facilities have been built to house such radiation sources. In these sources, particles (most commonly electrons) are accelerated and injected into large storage rings in *ultra-high vacuum* (UHV) where they move at relativistic velocities in cyclical orbits. Inside the rings, the electrons are held in orbit by a combination of quadrupole and bending magnets, causing the electrons to be accelerated towards the center of the rings and thereby emit *synchrotron radiation* (SR) as a form of bremsstrahlung tangential to their orbit. By a combination of optics and precision slits, the SR is led to the various experimental stations and focused onto the samples, this often being referred to as a beamline.
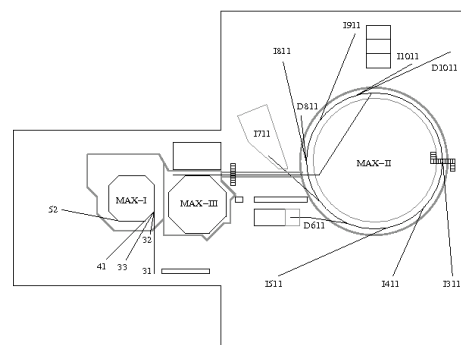

Figure 10: Schematic overview of MAXLAB, showing the different storage rings and beamline end-stations. Image from ref. [14].

In the present work, XPS was employed as a complementary analytical tool in order to investigate what oxides reside on the surface of the samples as well as their concentration and chemical state and what really happened to said oxides during cleaning.

4 Experimental Procedure

Before any actual STM measurements can be carried out, there is a lot of preparation to be done, and as with any UHV environment, this takes an awful lot of time. This section will describe the various preparations required for both the STM system and the samples studied throughout this thesis.

4.1 Preparation of the STM and its UHV environment

Throughout this thesis, a commercial *Omicron VT XA STM* was used. The STM system was operated at room temperature and all imaging experiments were carried out at a base pressure of $< 1 \cdot 10^{-11}$ mbar. In order to maintain such a UHV, the system uses a series of valves to separate the different sections and various turbo pumps to pump out each section individually. Furthermore, the entire system is also occasionally baked out by wrapping everything up in sheets of aluminium foil and heating tape, heating the entire steel casing of the STM system to $\sim 100°$ C. This will cause a majority of oxides and other impurities such as water that has stuck to the interior of the chambers to evaporate, allowing it to be pumped out and thus reduce the chamber pressure even further.

Due to the high dependence on the quality of the tip, they had to be carefully produced and prepared. The tips used in the STM were atomically sharp metal tips made out of Tungsten (W) wire of 0.38 mm diameter, produced in-house *ex-situ* through a well renowned method of electrochemical etching [15, 16]. However, as a natural side effect of the etching process, the tip is coated with a layer of the tungsten oxide WO_3 [16], which is later removed *in-situ* by sputtering the tip with high-energy Ar^+ ions. The quality of the tip was generally investigated by scanning a sample of pure gold (Au), which should exhibit a rather particular zig-zag pattern of atoms caused by a reconstruction of the surface known as a *herringbone reconstruction* [17].

The tips themselves are attached to special *Omicron* tipholders, introduced into the STM chamber to rest on a tripod scanner consisting of three independent piezoelectric elements. This construction allows for the replacing of tips without ever venting the system.

However, due to the extremely small tip-sample separation required during the actual scanning, proper vibrational isolation from both acoustic and mechanical sources is essential
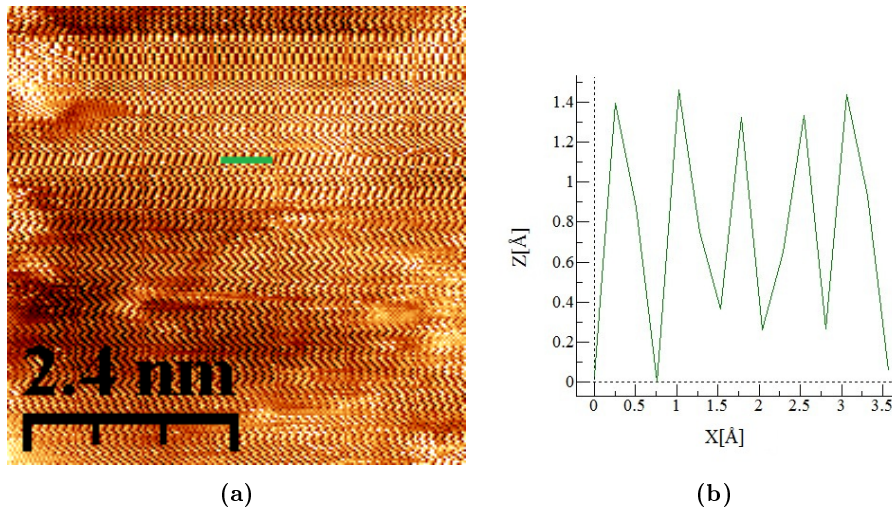
<div align="center">(a)   (b)</div>

Figure 11: The herringbone reconstruction of Au(111) is shown in (a), along with a profile diagram of the marked line in (b), revealing the incredibly periodic spacing of the atomic rows.

for both the quality of the images and the sustainability of the atomically sharp tips. To meet these requirements, the STM system was positioned on a table with built-in dampening to account for external, mechanical vibrations such as the turbo pumps maintaining the UHV. In addition, the STM itself contains an independent stage where the tip and sample are located, held in place by a combination of a spring system and an eddy current vibration isolation system. With permanent magnets mounted equidistantly along the STM frame, a certain magnetic flux will be introduced through the copper brackets on the STM stage. Faraday's electromagnetic induction law then claims that the eddy currents induced in the copper brackets will give rise to a magnetic field of their own, working to minimize the effect should the external magnetic flux ever change due to e.g. vibrations, essentially dampening the entire system. Together, this allows for STM operation even under non-ideal conditions.

4.2 Sample Preparation

All the wafers studied throughout this thesis were industrially produced by *WF Wafer Technology LTD* [18]. Further, all samples were manually prepared in-house *ex-situ* by cutting off segments of the wafers with a diamond cutter, and later applying the segments onto special *Omicron* sample plates using melted indium (In) as an adhesive. These wafers were also cut in various crystal planes depending on which facet were going to be studied, as is shown in fig. 12.
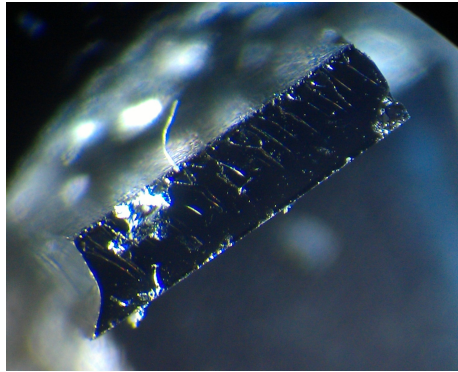
Figure 12: Image of a piece of GaSb(100) taken through an optical microscope, and positioned edge-on using scrap metal as a support. This way, the facet which will be studied is actually GaSb(110).

All nanowires presented in this thesis were locally grown at the *Nanometer Structure Consortium* at Lund University by S. Lehmann. The nanowires were prepared using either of two rather simple techniques, the first referred to as the *clean room wipe transfer method*, where the nanowires are broken at their base by a lint-free cloth and subsequently transferred onto the sample substrate, typically consisting of the same material as the nanowire itself to simplify the deoxidation process as well as to keep a reference surface close by. The second method, and perhaps the most advocated, is the s.c. *close proximity transfer method* (CP). Although the basic idea is the same, the transfer is carried out by gently pushing the substrate sample onto the actual growth sample directly, thus minimizing the potential risk of nanowires bundling together. Using this method, it is possible to maximize the density of nanowires on the sample while hopefully orienting them horizontally in the same direction, all at the same time. These two criteria should be fulfilled in order to simplify the scanning process, as individual nanowires would otherwise be very hard to locate.

As mentioned earlier in the report, the surfaces of materials are generally completely coated with contaminations and native oxides, preventing the application of STM measurements on said surfaces. Depending on the oxides, their low conductivity may prevent a high enough tunneling current to reach through to the sample, thus endangering the tip as it would attempt to move closer to the surface. In order to prevent such a disaster, various methods can be employed which clean the surface of the material. Once clean, the samples must then be kept in an UHV environment at all times, as they will otherwise degrade very rapidly.
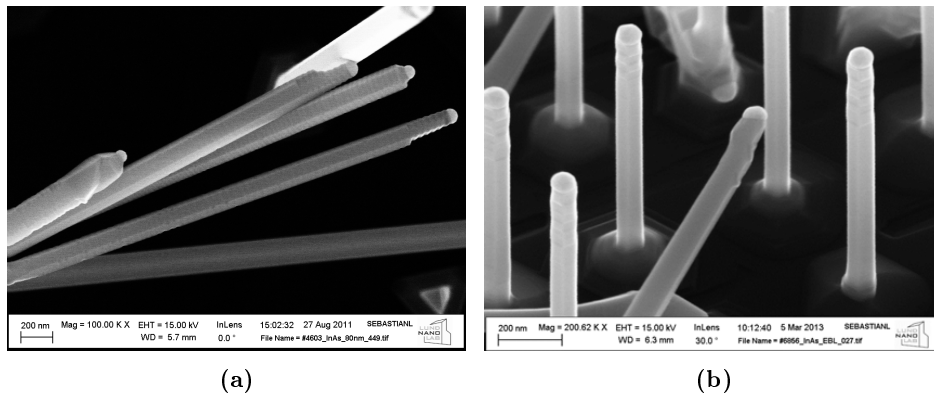
(a)   (b)

Figure 13: SEM images of The two different batches of InAs nanowires studied during the present work. (a) shows the overgrown nanowires, mainly consisting of (110) side facets while (b) shows nanowires with segments of zincblende on a wurtzite stem, narrowly visible as wrinkles towards the top of the wires.

4.2.1 The Art of Cleaning

All samples presented in this thesis were cleaned *in-situ* in the UHV environment, this to ensure that the samples maintained a high structural quality and remained free of impurities for a sufficiently long time to carry out all the necessary measurements. The two most conventional methods of cleaning samples are either by sputtering, as employed to the tungsten tips, or thermal heating. However, sputtering with e.g. high-energy Ar^+ ions would completely rip apart both the sample substrate and the nanowires alike, rendering it next-to impossible to conduct STM measurements. Thus, thermal annealing of the samples is the only plausible option.

The principle at work behind thermal annealing is simple enough: heat the sample to sufficient temperatures required for the oxides on the surface to desorb. Unfortunately, reality is seldom as straightforward as one would like, as the temperatures required to desorb certain oxides would also evaporate the substrate itself. Luckily, this can be avoided by exposing the surface oxides to atomic hydrogen while moderately heating the sample. This will cause the oxides to react with the hydrogen and form molecules with lower desorption energy barriers, allowing for desorption of the oxides at temperatures which will not destroy the substrate.

Undoubtedly the most utilized method during the present work was to crack hydrogen gas molecules into atomic hydrogen. Using a commercial *GmbH HABS 40-AS* [19] hydrogen source, a tungsten filament was heated to approximately 1700° C in order to break the atomic bonds in a hydrogen gas of 99.99% purity. The temperatures of the hydrogen

source and the sample were monitored with a *K-type thermocouple* and a *Cyclops infrared pyrometer*, respectively. The intake of hydrogen radicals on the surface was approximated using the partial pressure in the chamber and the source efficiency table, following a cleaning recipe that has been previously proven to work **[20, 21, 22]**. Further, the hydrogen radicals should have a kinetic energy low enough only to react with the actual surface, thus ensuring that no contaminations will be incorporated in the samples.

A second source for producing hydrogen radicals was explored as well. Instead of letting the gas flow through a heated filament, the instrument uses a *radio frequency* (RF) signal to form a plasma out of the gas. This should in theory yield a greater flux of radicals. However, the turbopump alone did not pull enough gas through the source to ignite a plasma, and since there was no differential pump mounted on the STM system, the project had to be shut down.

(a)   (b)

Figure 14: An *SVT associates RF 2.75* **[23]** plasma source lies disassembled in (a), revealing the thick copper coil where the RF signal is passed through during operation. When the plasma is ignited, a distinct glow will be emitted from within the source, as can be seen in (b). The color of the glow depends on the gas, whereat argon (Ar) was used during testing of the plasma source.

Alternative methods capable of cleaning sample surfaces are that of chemical etching, which was attempted once during the present work but alas was unsuccessful. A final, albeit more unorthodox way of "cleaning" the sample is to actually break the wafer along the desired crystal facet *in-situ* in UHV, thus never actually exposing the surface to any contaminations in the first place. This is a good way to obtain benchmark surface images of what a successfully cleaned sample should look like.

5   Results and Discussion

When performing a complete STM imaging, each region of the sample surface is actually scanned four times in total. Once upwards and once downwards, as well as scanning every line both forwards and backwards. One of the many advantages of such a thorough probing of the surface is the possibility to compare the various images. This way, it is possible to identify if potential anomalies are caused by the tip or the electronics rather than being a misleading characteristic of the sample. The only downside would thus be that STM imaging is a rather time-consuming process.

All the images are later processed using *SPIP*, *WSxM* [24] and *Adobe Photoshop CS6*. These softwares all contain several filters which can be applied in order to reduce noise and sharpen important features which otherwise might be hard to distinguish. Another very useful tool in both *SPIP* and *WSxM* is the option to correct for a tilted sample automatically by flattening the image. Further, distances and height differences can be determined directly and Fourier transforms were applied in order to make out repetitive structures such as atomic rows.

The images are presented as a translation of the measured tunneling current as a function of the tip position into different colors. Dark parts would thus represent lower parts of the surface, i.e. the tip had to approach in order to maintain a constant current, whereas bright parts would be the opposite. Note that the color of the images are not that of the actual surface, but only a graphical addition to enhance details.

5.1   InAs

Three different crystal planes of InAs were studied throughout this thesis: InAs(111)A, InAs(111)B and InAs(110). Although identical in crystal structure, the A or B suffix denotes whether its indium atoms or arsenic atoms left on top when the surface is cut. InAs is made up of a zincblende structure, which means a superposition of two face-centered cubic structures positioned in a tetrahedral coordination, each made up of either indium or arsenic atoms. This way, each atom will be surrounded by four atoms of the opposite type.

5.1.1   InAs(111)A

InAs(111)A consists of indium atoms on top, acting as the *p*-side of the semiconducting compound, and thus contains a lot of empty electronic states [25]. It might therefore be encouraging to image the surface using a positive sample bias, however no such measurements could be carried out in a stable manner. The cause of this instability is still uncertain, but is believed to be a combination of non-optimal vacuum and an imperfect tip. Instead, all measurements were conducted using a negative sample bias, thus probing the filled electronic states of the arsenic atoms positioned one atomic layer below the surface.

This sample was cleaned a total of three times using atomic hydrogen before any surfaces void of oxides could be found. The parameters used for all three cleaning cycles were the same: the sample was heated to $380°$ C and for 20 minutes exposed to the hydrogen radicals at a chamber pressure of $2 \cdot 10^{-6}$ mbar, up from a base pressure of $2 \cdot 10^{-8}$ mbar.

Fig. 15(a) shows an overview image of the surface topography, taken using a sample bias of $V_g = -1.3$ V and a constant tunnelling current of $I_t = 130$ pA. It is worth noticing that there are several atomic layers as well as no sharp edges on said layers. From the overview image alone, there are clearly flat areas of the surface, thus allowing for an even closer look. Fig. 15(b) shows such an image, taken using a sample bias of $V_g = -2$ V and a tunnelling current of $I_t = 170$ pA, the increase in tunneling current indicating that the tip is now moved closer to the surface. The instabilities and/or bright spots along the edges of the atomic layers indicate remnants of adatoms still stuck to the dangling bonds.
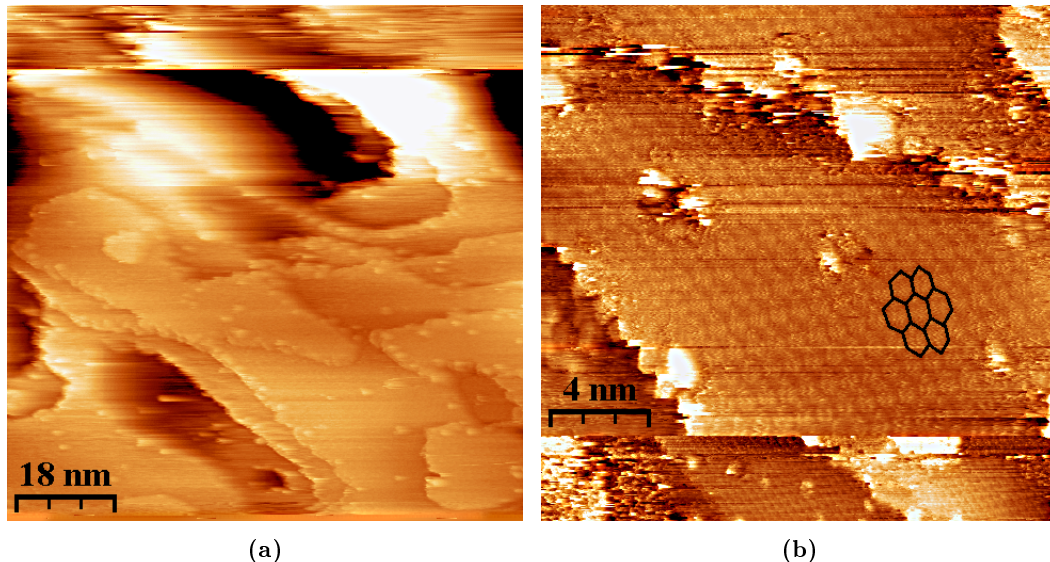

(a)   (b)

Figure 15: STM images of InAs(111)A. (a) 91×91 nm^2 overview image. (b) 20×20 nm^2 flat region from the same area.

In fig. 15(b), some kind of structure can be identified as a spatially repeated hexagonal pattern as indicated by the marked lines, although it appears slightly shifted. The lattice constant of InAs should be $a = 0.605$ nm at 300 K [26]. Through Pythagora's theorem, the distance between two atoms along the same face-diagonal is thus expected to be $d = a(\sqrt{2}/2) = 0.428$ nm. Measurements made implies that the distance between two adjacent peaks is vaguely 0.9 nm in every direction, i.e. twice as long as the expected value. A very plausible explanation for this would be a (2×2) reconstruction of the surface [27]. Such a reconstruction is illustrated in fig. 16. The actual cause for this reconstruction is as of yet uncertain, but is believed to be related to the annealing temperatures used during cleaning.
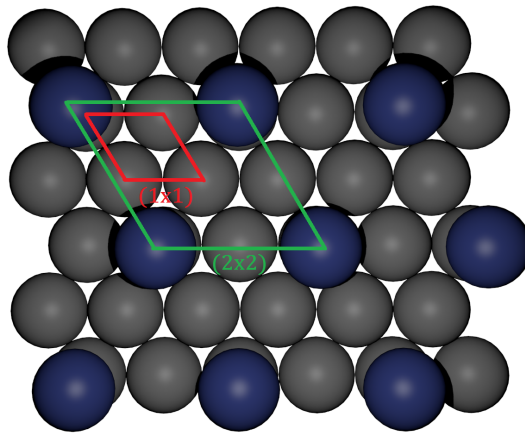

Figure 16: The (2×2) reconstruction of (111) surface layer along with the (1×1) bulk atoms.

5.1.2   InAs(111)B

Contrary to its twin, InAs(111)B consists of arsenic atoms on top, acting as the n-side of the semiconducting compound, and thus contains a lot of filled electronic states. Scanning with a negative sample bias, the contours of the surface topography is therefore believed to appear a lot sharper than for InAs(111)A.

Fig. 17(a) shows the InAs(111)B surface after a single cleaning cycle at 390° C for 30 minutes at a chamber pressure of $2 \cdot 10^{-5}$ mbar. It is impossible to draw any conclusion whatsoever of the sample other than it is heavily oxidized. After two further cleaning cycles totalling 90 minutes at the same pressure and temperature as before, the surface as seen in fig. 17(b) could be observed. The image was taken using a sample bias of $V_g = -2.6$ V and a tunneling current of $I_t = 80$ pA.
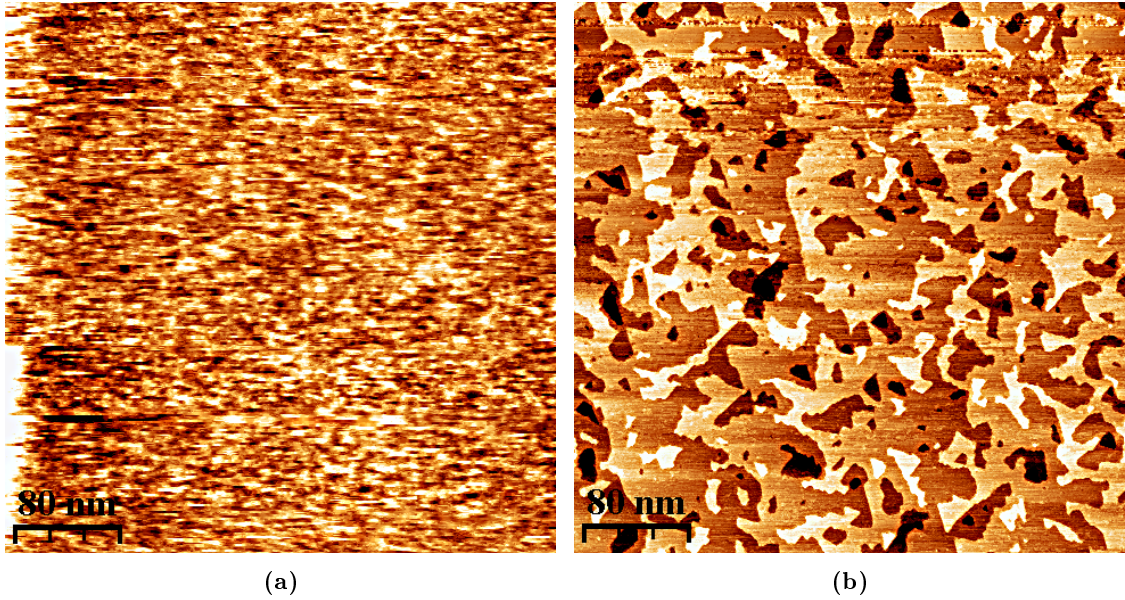
Figure 17: STM images of InAs(111)B. (a) A heavily oxidized $400 \times$ 400 nm^2 surface. (b) The same 400×400 nm^2 surface after being cleaned.

Sharp edges and very well defined angles of 60° can be seen, especially in fig. 18(a). Despite a lot of steps, the surface generally appears very flat, as the steps themselves have been concluded to be mono-atomic by observing the profile diagram in fig. 18(b). The image was taken using a sample bias of $V_g = -2.4$ V and a tunneling current of $I_t = 100$ pA.

However, no atomic resolution was ever achieved on the InAs(111)B surface. This may be a consequence of the surface being reported as unreconstructed after prolonged annealing [28], thus requiring pristine conditions in order to image the individual atoms, which is even further hampered by the many atomic steps. Due to its unreconstructed surface, wafers of InAs(111)B act as stable substrates for, amongst other things, nanowire growth.
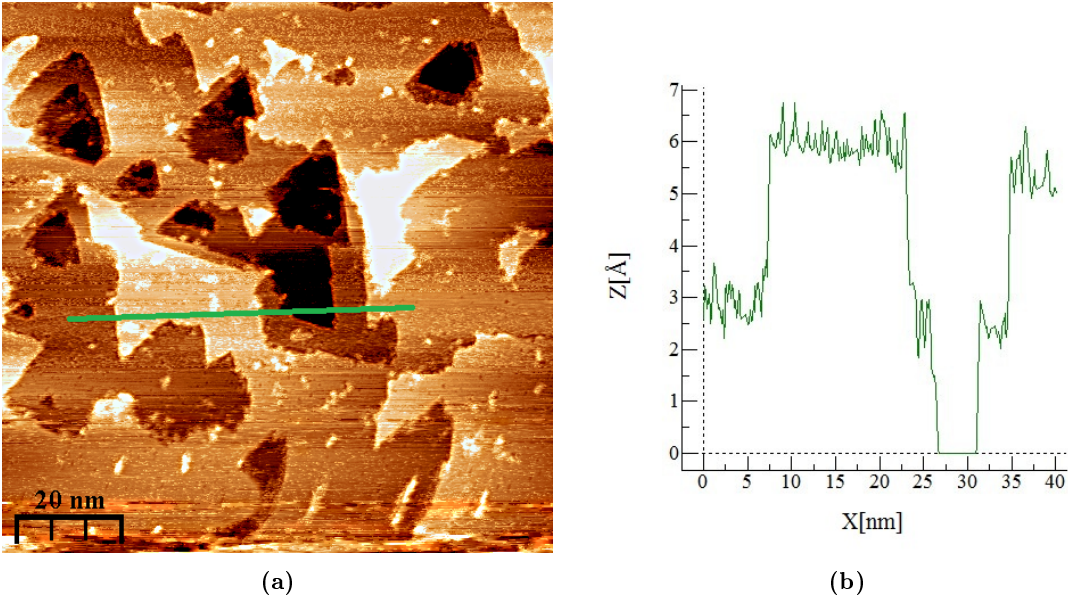
Figure 18: (a) A 100×100 nm^2 STM image of InAs(111)B. (b) A profile diagram of the marked line in (a).

5.1.3 InAs(110)

Being the crystal plane with the lowest total surface energy, the InAs(110) surface is the most likely to form whenever the wafer is cut. By following the same procedure as previously illustrated in fig. 12, a segment of InAs(111) was positioned edge-on *ex-situ* with proper support to prevent the sample from falling over during cleaning and transfer. Two different samples of InAs(110) were studied throughout this thesis, and each will be covered separately.

Unfortunate for one of the samples, the primary atomic hydrogen source were on a trip to Brookhaven, US, which led to a backup source being used for the time being. After a grand total of five cleaning cycles summing up to 210 minutes, each at a temperature of $380°$ C and a chamber pressure of $2 \cdot 10^{-5}$ mbar, the surface as seen in fig. 19(a) could be observed. The cracking efficiency of the backup source is believed to be much lower than that of the primary source, thus the additional time required in order to clean the samples. Imaged using a sample bias of $V_g = -2.4$ V and a tunneling current of $I_t = 240$ pA, a closer look on the apparent islands was subsequently carried out using a sample bias of $V_g = -2$ V and a tunneling current of $I_t = 260$ pA. There is little to no need of using the various heigh diagrams to conclude that the islands are mono-atomic, formed as a result of the atomic hydrogen cleaning. The closer look on the islands in fig. 19(b) reveals that bright lumps are gathered along the edges of every island, indicating some stubborn adatoms getting caught

in the dangling bonds. Keep in mind that the bright spot does not necessarily indicate that there is a local elevation of the sample surface, but only the electronic structure in those places are vastly different than the surround surface, resulting in peaks in the measured tunneling current.
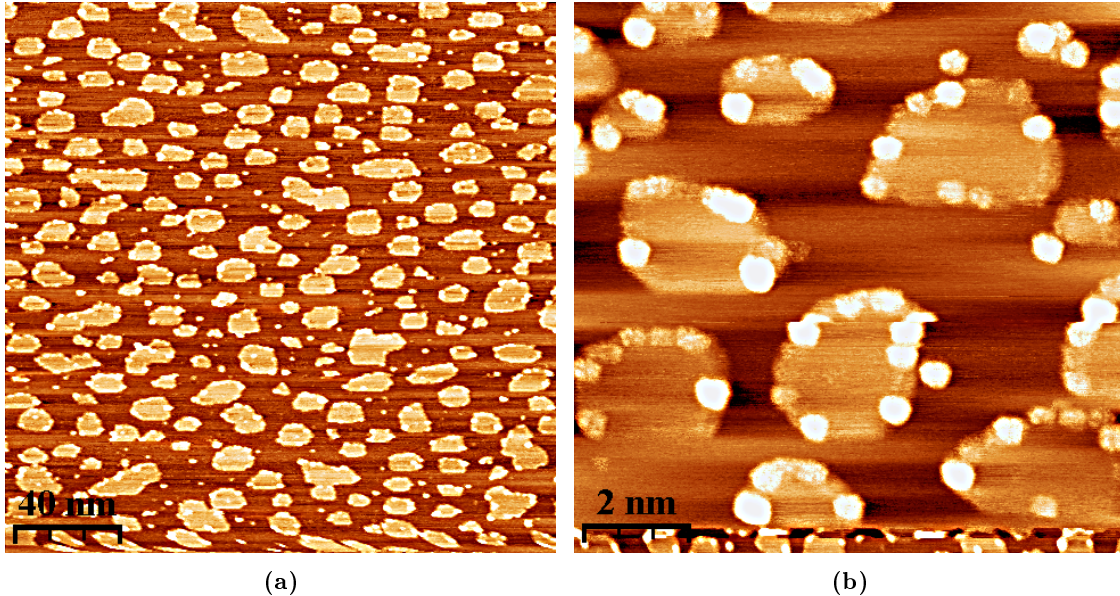

(a)   (b)

Figure 19: STM images of InAs(110). (a) A 200×200 nm^2 overview. (b) A 50×50 nm^2 zoom on the islands in (a).

After a sixth and final cleaning of this sample had been completed using the same parameters, a tragic truth was confirmed by observations made in fig. 20. A mono-atomic layer of the surface had been peeled off by the cleaning process, but alas the contaminations represented by the bright dots remained scattered throughout the surface. It then became clear that these were no ordinary adatoms, but small chunks of tungsten (W) ripped off from the filament used to crack the hydrogen gas into radicals. They had most likely been emitted onto the sample during the first cleaning attempt, as the source had not been used for a while.

Despite the contamination of tungsten, the surface is extremely flat and well behaved, as further illustrated in fig. 21(a) and fig. 21(b), both imaged using a sample bias of $V_g = -3$ V and a tunneling current of $I_t = 250$ pA. However, no atomic resolutions could be attained due to the contamination.
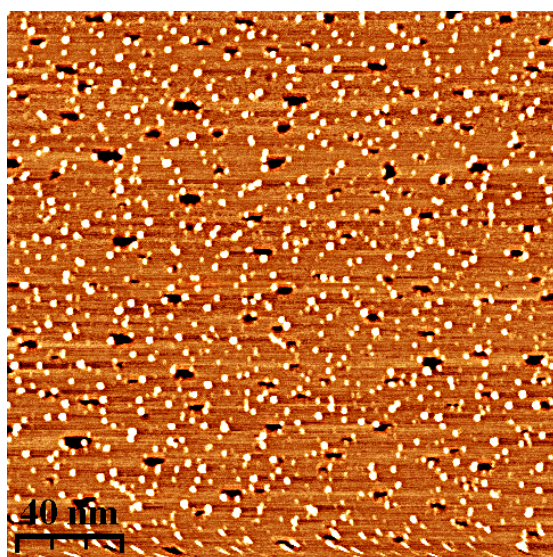
Figure 20: STM image of InAs(110). This 200×200 nm^2 image confirmed the presence of a tungsten contamination. The bright dots remained and kept moving on the surface despite several layers of the material being desorbed.
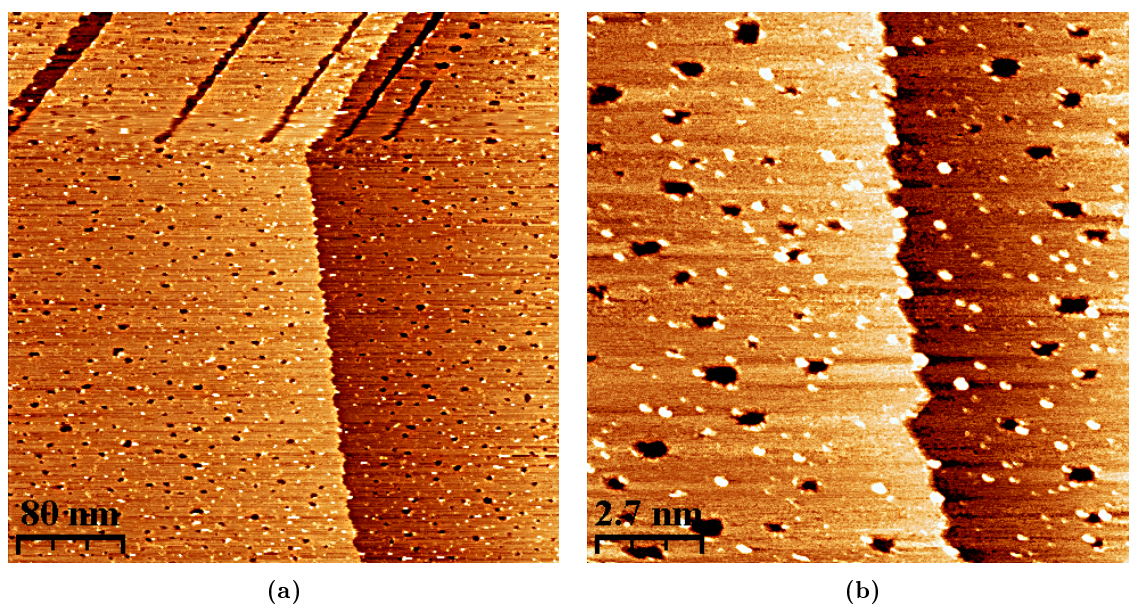

(a)   (b)

Figure 21: STM images of InAs(110). (a) A 400×400 nm^2 overview with several mono-atomic gorges towards the top of the image. (b) shows a 100×100 nm^2 closer look at the region where the sample surface appears just as if it was bent.

The second sample of InAs(110) was investigated under much better conditions as the STM system had just before been baked out completely. A single 20 minute cleaning cycle using the primary hydrogen source at a temperature of 385° C and a chamber pressure of $2.2 \cdot 10^{-6}$ mbar was enough to clean the sample. Imaged using a sample bias of $V_g = -2.9$ V and a tunneling current of $I_t = 60$ pA, fig. 22(a) shows an extremely well behaved surface consisting of a series of joined mono-atomic islands resembling those seen in fig. 19(a). The fact that these islands are still joined might indicate that the cleaning cycle was halted in the middle of the formation of a single layer. A section of the overview image was subsequently investigated more thoroughly as seen in fig. 19(b), imaged using a sample bias of $V_g = -2.5$ V and a tunneling current of $I_t = 100$ pA.
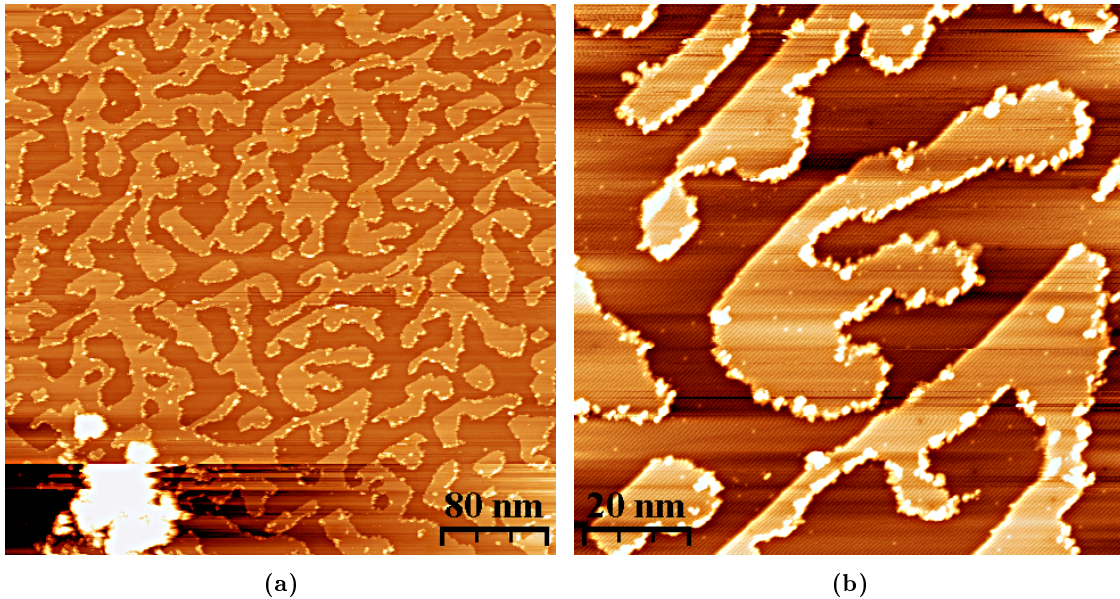

80 nm

20 nm

(a)   (b)

Figure 22: STM images of InAs(110). (a) A 400×400 nm^2 overview of the surface topography. (b) A 100×100 nm^2 closer look at the F-shaped island towards the middle of the image shown in (a).

The observant reader might also notice that atomic rows can be resolved in fig. 19(b) even at such a large scale as 100×100 nm^2, with both the higher and lower layer rows going diagonally in the same direction. Further, only the edges of the islands which do *not* align with the atomic rows exhibit the bright spots typically related to adatoms. It is therefore likely that they are missing some neighboring atoms, resulting in dangling bonds. Given the next-to ideal circumstances, the atomic rows can be studied by further zooming onto the surface. Imaged using a sample bias of $V_g = -2$ V and a tunneling current of $I_t = 200$ pA, fig. 23(a) reveals a clear view of the diagonal atomic rows.
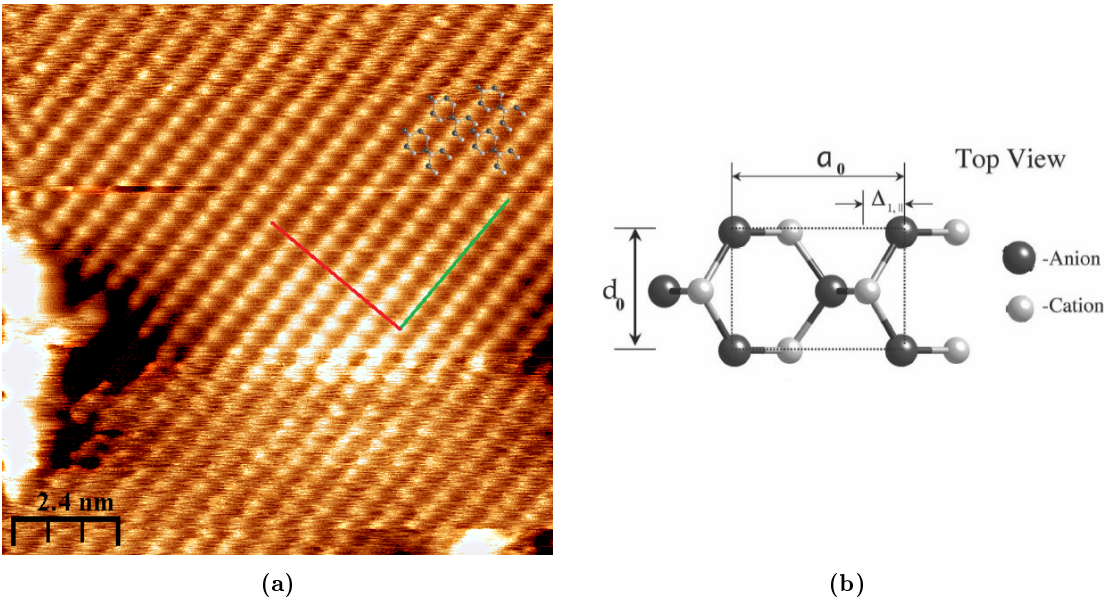
(a)   (b)

Figure 23: (a) A 12×12 nm^2 STM image of one of the InAs(110) islands from fig. 22(a). (b) A top view of the surface unit cell. Note that the anion-cation-pairs in the middle of the unit cell are positioned one atomic layer down from the surface. Image from ref. **[26]**.

In order to make sure that the sample surface is actually behaving as it should, its lattice constant a can be measured and compared with confirmed values. For clarification, the lattice constant a as well as the distance between two adjacent atoms along the same row d is shown in fig. 23(b). Here, the In atoms are denoted as cations and the As atoms as anions, and since the image was scanned using a negative sample bias, only the As atoms should be clearly visible. Due to this, it is sufficient to see the (110)-plane of the InAs zincblende structure as that of an ordinary FCC lattice consisting solely of As atoms, hence the rectangular unit cell. As established earlier, the lattice constant of InAs is $a = 0.605$ nm at 300 K and the distance between two adjacent atoms along the same row is $d = 0.428$ nm.

In choosing an arbitrary chain of atoms and rows as illustrated by the green and red line, respectively, it indeed appears to behave as expected. The green peaks line up with the red approximately every 4th atom. The measured lattice constant averages $a = 0.597 \pm 0.022$ nm while the distance between two adjacent atoms along the row averages $b = 0.439 \pm 0.022$ nm. Hence, the measured values fit rather well with the expected ones, with a deviation of roughly 1.3% and 2.6%, respectively. Experimental and theoretical values are thus in a good agreement, confirming that the (110)-plane is obtained by positioning the (111)-plane edge-on.
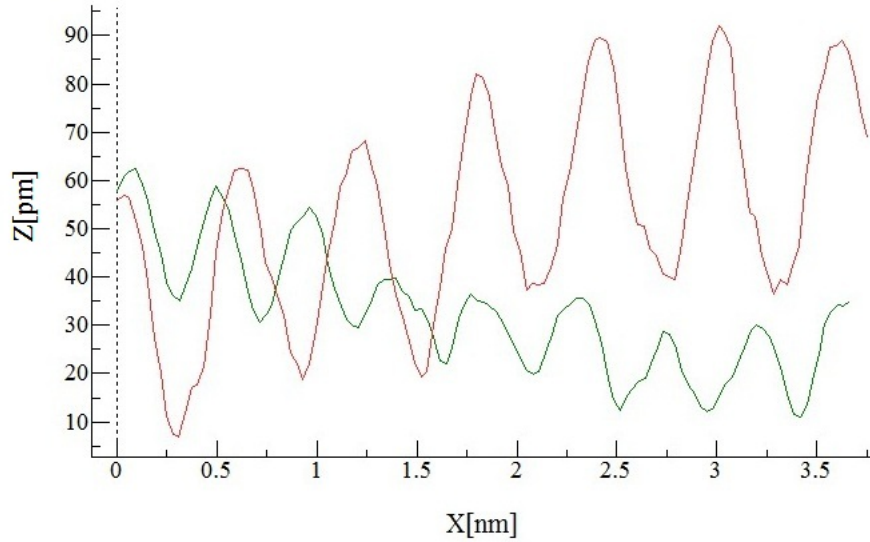
Figure 24: Merged profile diagram of the two marked lines in fig. 23(a).

5.2   GaSb

One of the longterm aims of the experiments conducted in this thesis is for the application of nanowires consisting of *both* InAs and GaSb. As motivated earlier, these nanowires must first be confirmed completely free of oxides before any electrical properties are deduced. This means that both the InAs and the GaSb part should clean through the same procedure, independent of facets. So far, entire wafers of various InAs crystal planes have been confirmed clean through the exposure to atomic hydrogen. However, as will soon become apparent, properly cleaning GaSb is no mean feat.

Imaged using a sample bias of $V_g = -2.9$ V and a tunneling current of $I_t = 60$ pA, fig. 25(a) shows a typical GaSb(100) surface, clad with oxides littered on the surface in a chaotic manner. Even the GaSb(110), which is said to be more stable with respect to variations in the surface potential, could not be cleaned properly using the parameters for InAs, as shown in fig. 25(b).

After a long series of futile attempts, it was decided to search for an upper limit regarding temperature and chamber pressure during the cleaning cycles. The first sign whatsoever of a flat surface was found after cleaning at a temperature of 480° C for 30 minutes at a chamber pressure of $2 \cdot 10^{-5}$ mbar, as can be seen in fig. 26(a). Unfortunate for the current purpose however, the temperatures required to desorb the gallium oxides would likely destroy the InAs surfaces in the process. Exposure to atomic hydrogen under similar temperatures has been claimed to clean the surface of GaSb(100) before [29].
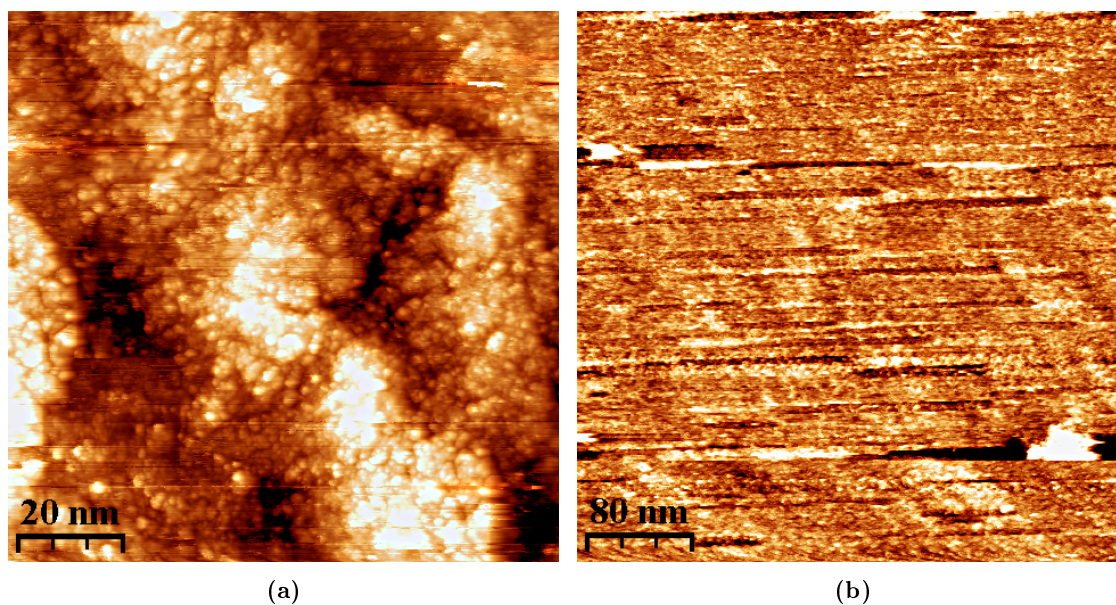
(a)　　　　　　　　　　　　　　(b)

Figure 25: STM images of GaSb(100), both showing oxidized surfaces without any noticeable structure. The (100) plane is shown in (a) and the (110) plane in (b).
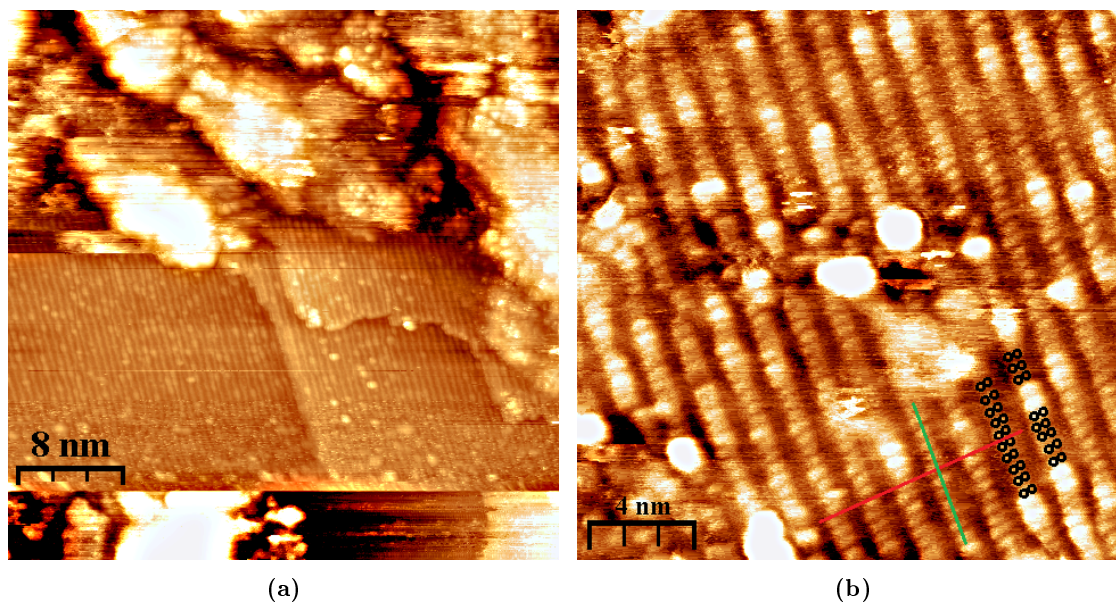

(a)　　　　　　　　　　　　　　(b)

Figure 26: STM images of GaSb(100). (a) Although just a small patch of 40×40 nm^2, the surface of the material can be seen free of most oxides. (b) A 20×20 nm^2 image of the same area. Dimers are illustrated as the paired black circles.

In some cases, the reconstruction of a surface may result in batches of atoms reforming as *dimers* or *trimers*, being a collection of two or three atoms, respectively. As a starting point, one could thus assume that GaSb behaves like the extensively studied GaAs. That is, *dimers* of either gallium or antimony may form upon reconstruction of the surface, resulting in the formation of the elongated atomic rows as seen in fig. 26(b). Using the same argument as for InAs, scanning the images with a negative sample bias will most likely result in only the antimony atoms being seen in the images. The (100)-plane of the GaSb zincblence structure can thus be expressed as the side of an FCC unit cell consisting solely of Sb atoms, exhibiting a quadratic formation. The lattice constant of GaSb has been found to be $a = 6.10$ nm at 300 K [30], hence a distance between two adjacent atoms along the face-diagonal is expected to be $b = a(\sqrt{2}/2) = 0.431$ nm.

The proposed structure will thus be that of dimers making up the rows, as similar reconstructions has been observed for GaAs several times before [31]. The spacing of these rows, measured using the profile diagram in fig. 27(a), averaged $a = 1.297 \pm 0.024$ nm while the distance between two adjacent dimers averaged $b = 0.444 \pm 0.024$ nm. Even though a few groups have reported GaSb(100) to reconstruct as (1×3) [32], the current measurements hints of a (1×2) reconstruction of the surface.

(a)   (b)
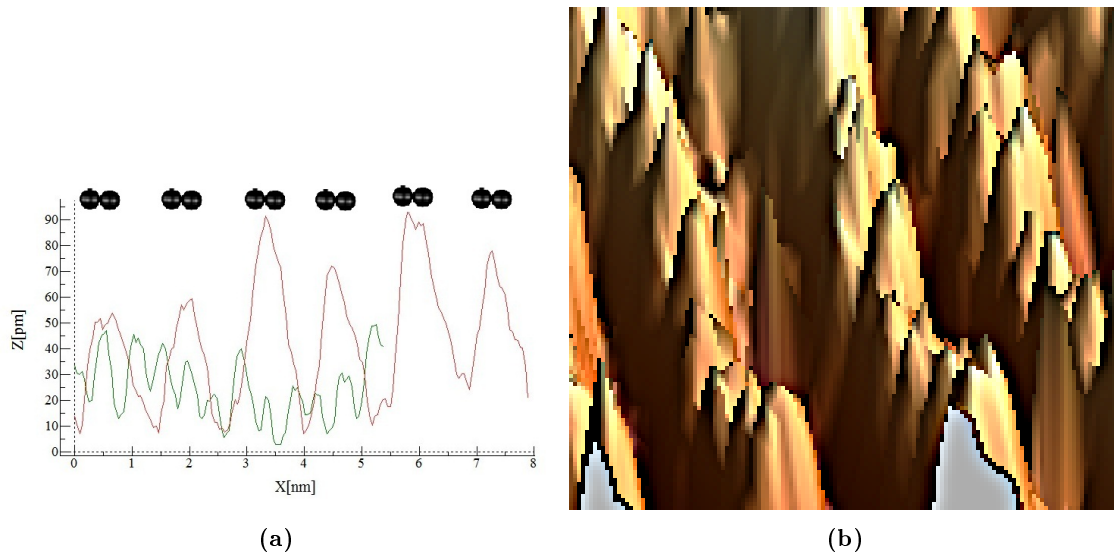
Figure 27: (a) Profile diagram of the marked lines in fig. 26(b). (b) 3D representation of a segment from fig. 26(b). Unfortunately not the sharpest image, however, the individual peaks of each dimer can still vaguely be distinguished.

Considering the width of the dimers, any measurement with the current resolution will at best be a rough approximation. From both the profile diagram and the 3D representation in fig. 27, it does not seem unreasonable to fit yet another pair of dimers in between. This would then result in the scenario illustrated in fig. 28.
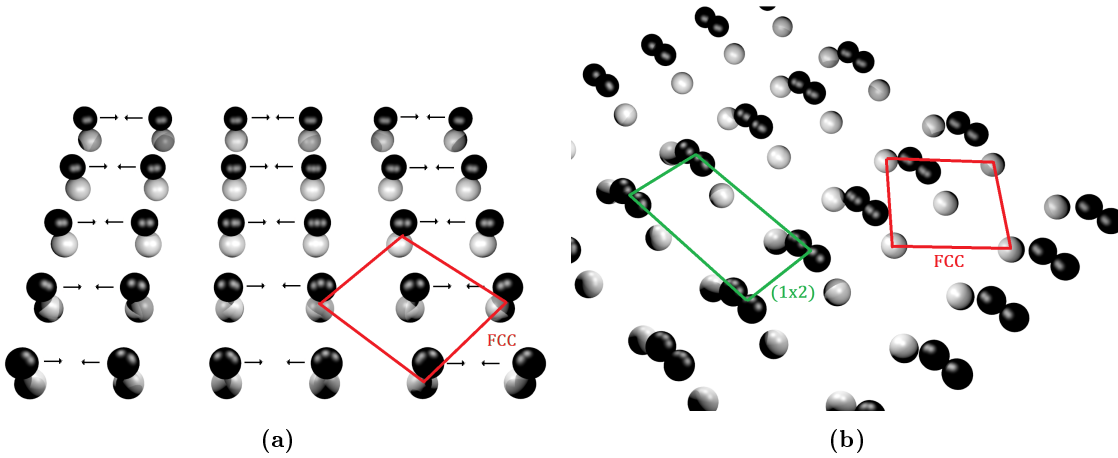

Figure 28: (a) Rough illustration of how the GaSb(100) surface layer reconstructs. (b) In the same manner, a rough illustration of the STM image shown in fig. 26(b). Note however that the images are only an approximation, and that the first few sub-surface layers most likely also show some kind of configuration, although it is very hard to deduce with the current data.

In an attempt to improve the current measurements, the surface of the sample was unfortunately ruined instead. This was most likely caused by a significant desorption of the Sb on the surface caused by the high temperature, resulting in the formation of Ga droplets. No further high-temperature cleaning cycles were performed during the present work.

Instead, Vael *et al.* **[32]** proposed a 2-step cleaning process in order to rid GaSb(100) surfaces of oxides even under temperatures which would not ruin the InAs samples. They claim that after exposing the surface to atomic hydrogen at a temperature of 100° C, all antimony oxides should have desorbed and only the gallium oxides remained on the surface. These were later removed in a second cleaning at a temperature of 300° C. The claims were backed up with a series of LEED images of the surface, where a structural pattern could be observed and should indeed only be visible if the surface itself is sufficiently clean. This peaked interest as it would solve the current issue regarding the temperatures otherwise required to clean GaSb. However, any attempts in reproducing clean surfaces using said method have so far been unsuccessful.

5.3   MaxLab Data

The 2-step cleaning process proposed by Vael *et al.* **[32]** was further investigated during the beamtime at MaxLab in Lund, where the application of XPS allowed for detailed probing of which oxides remained on the surface after each cleaning.

All data obtained through XPS measurements at beamline I311 were returned to the division for further processing. The data was stored as a long series of digits and must first be imported and plotted before any analysis could be performed. For this purpose, a custom program in MATLAB was created along with a user-friendly GUI which enabled the data from subsequent cleaning cycles to be compared directly. Additionally, the various elements probed using different photon energies could be accessed independently via a drop-down window.

Since the incident photon beam hits the sample at a significant angle, it must first be properly aligned in order to maximize the amount of registered photoelectrons. Once a maxima is located, sweeping the electric field between the plates of the previously mentioned HSA, allowed for the construction of a photoelectron energy spectrum of the sample. Such a spectrum can be seen in fig. 29, revealing all the elements currently present on the surface. Displayed on a logarithmic scale, it is clear that certain peaks dominate the spectrum. Using an online X-ray data booklet **[33]** containing the electron binding energies for all the relevant elements, table 1 was constructed.

Element	K 1s	$L_1 2s$	$L_2 2p_{1/2}$	$L_3 2p_{3/2}$	$M_1 3s$	$M_2 3p_{1/2}$	$M_3 3p_{3/2}$
6 C	284.2						
8 O	543.1	41.6					
31 Ga	10367	1299.0	1143.2	1116.4	159.5	103.5	100.0
51 Sb	30491	4698	4380	4132	946	812.7	766.4
Element	$M_4 3d_{3/2}$	$M_5 3d_{5/2}$	N_1 4s	N_2 $4p_{1/2}$	N_3 $4p_{3/2}$	N_4 $4d_{3/2}$	N_5 $4d_{5/2}$
31 Ga	18.7	18.7					
51 Sb	537.5	528.2	153.2	95.6	95.6	33.3	32.1

Table 1: Electron binding energies, in eV, for the elements relevant to this sample. Some binding energies are shown as a one-particle approximation, hence the same energy.
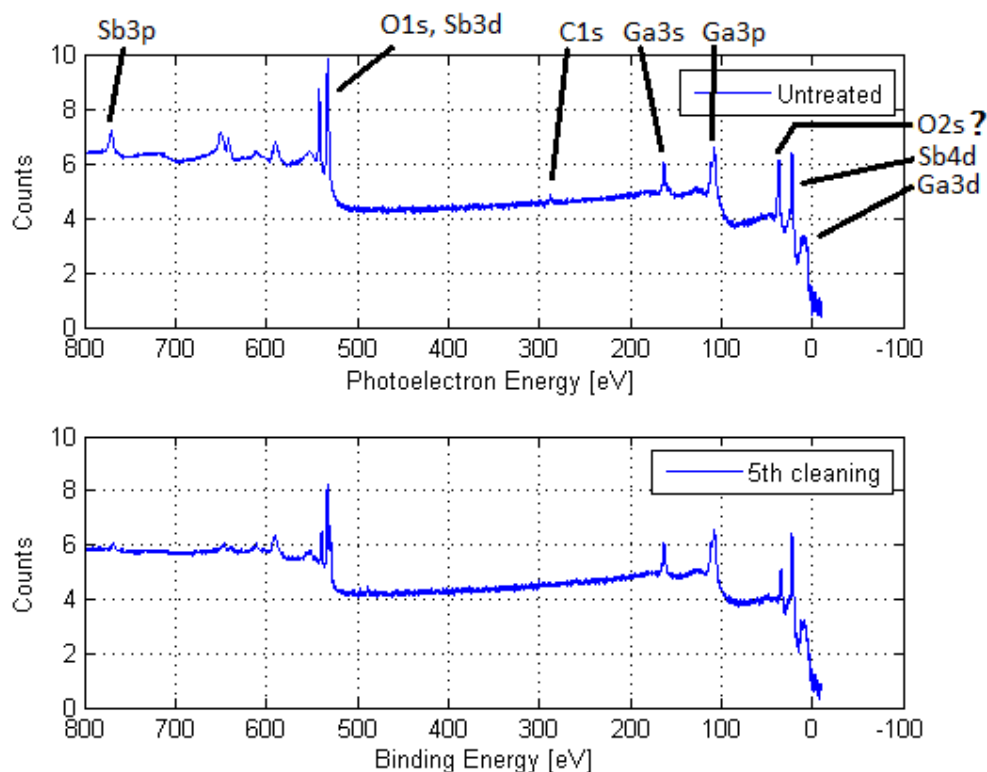
Figure 29: Photoelectron energy spectrum of GaSb(100) displayed on a logarithmic scale. The untreated surface spectrum is shown top while the bottom shows the same sample after five cleaning cycles. Both were registered using a constant photon energy of 1100 eV.

Using table 1, the dominant peaks in the overview spectrum could be identified, and have been marked accordingly. Most noticeable are the two oxygen peaks around 543 eV and 41.6 eV, as they have been reduced considerably. This implies that the cleaning at least partially works, and to what extent can be determined by further investigating the most prominent peaks in more detail. The unmarked peak around 650 eV could possibly be from traces of In3p$_{3/2}$ used as adhesive to keep the sample onto the sampleplate, while the peak around 590 eV is slightly harder to determine, as most elements whose binding energies match are relatively rare in nature and should not be present on the sample. Even though traces of carbon were expected and sought for, no evident peaks could be located. It is also worth mentioning that the scale on the x-axis is reversed due to photoemission convention.

In varying the energy of the photon beam and thus the surface sensitivity (still keeping it constant while sweeping, however), it is possible to move further out from a nucleus core, with lower energy photoelectrons being emitted from the out most shells. Hence it is

possible to make any core-level photoelectron surface sensitive by simply tuning the energy of the photon beam accordingly. Evidently, the most interesting energies with respect to surface studies are those at lower energies, as these are the ones containing oxides interfering with the STM measurements. In contrast, higher photon energies will probe even deeper into the material, but since the mean free path of the emitted photoelectrons is comparably short, the resolution will suffer. The mean free path of the photoelectrons, i.e. the average distance they will travel before inelastic scattering occurs, depends partly on their energy. It is also important to keep in mind that at lower binding energies further out from the nucleus, peaks of different elements might overlap into a superpositioned peak, as there is no way to separate the photoelectrons.

A closer look at the Sb4d peak registered using a photon beam of 320 eV reveals a time lapse of how the surface layers change, as shown in fig. 30. The untreated surface spectrum shows a huge peak around 36 eV, which from table 1 could be suggested as the O2s peak, however, apparently it tends to move around a lot. After the first cleaning, this peak is greatly diminished while the Sb4d peak slowly starts to emerge around 33 eV. After additional cleaning cycles, distinct traces of the peak around 36 eV can no longer be seen while the Sb4d peak keeps growing. However, looking at the overview spectrum after the same amount of cleaning, traces of the oxygen peaks remain. Instead, the peak which disappeared might have been a Sb4d spin-orbit doublet originating from Sb atoms surrounded by O atoms, which were subsequently removed.
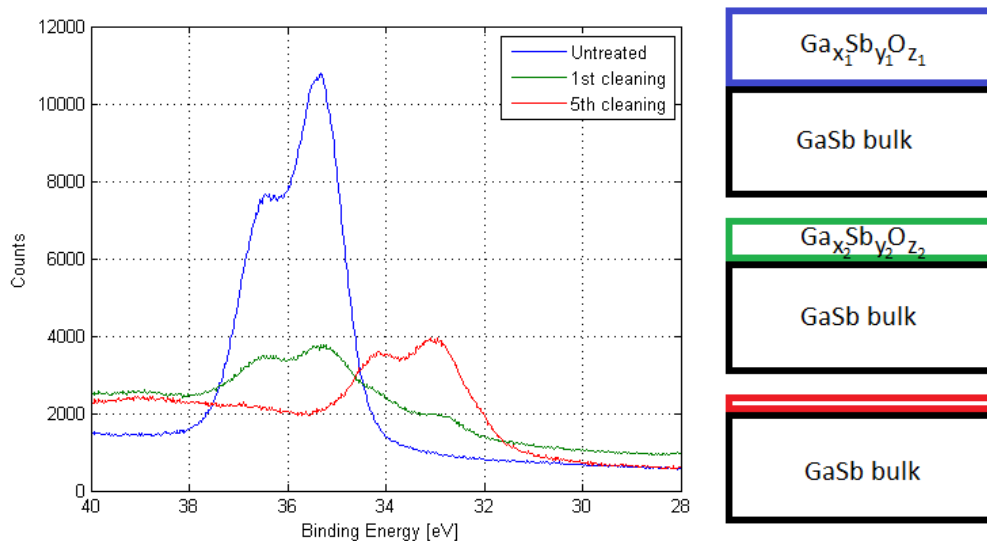

Figure 30: Merged diagram of the XPS measurements of the Sb4d peak along with a graphical illustration of how the surface layers change during cleaning.

This chain of events is further illustrated in the color-coded cross sectional images of the sample, where the oxide layers on top are repeatedly reduced. Similar results were reported by Vael *et al.* [32]. Note that the binding energies in table 1 typically is a few eV off, which originates from that the values were determined in gas phase experiments. The segmented apex of the peaks is actually caused by splitting of the electron energy levels due to their angular momentum, e.g. $4d_{3/2}$ and $4d_{5/2}$. This is recognized by two factors: the binding energy between the splittings is always constant and thus so are the photoelectron energy peaks, and the ratio between the two peaks is also constant.

Traces of this change can further be observed in the Ga3s peak registered using a photon energy of 1140 eV, shown in fig. 31. As previously mentioned, higher photon energy will allow for probing deeper into the nucleus, but due to the low mean free path of the photoelectrons, only those emitted from the very surface layers of the sample will be picked up by the detector. The sudden appearance of the core level Sb4s peak around 153 eV after the first cleaning implies that the abundance of Sb atoms on the surface has increased drastically, with the most probable explanation to why being the removal of oxides.
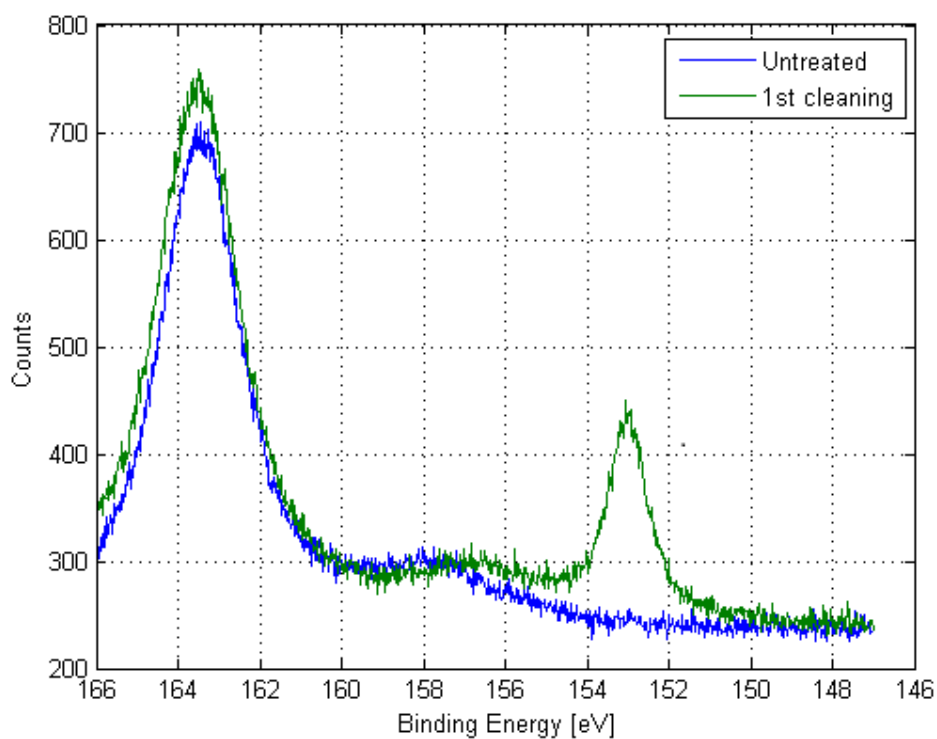

Figure 31:   Merged diagram showing the Ga3s and Sb4s peaks, respectively.

The evolution of the Ga3d spectrum registered at a photon energy of 70 eV can be seen in fig. 32. In a manner very similar to Sb4d, the peak around 23 eV is actually that of both GaO and Ga_2O_3 [32], with GaO positioned along the right slope. After the first cleaning, hardly any traces of Ga_2O_3 can be observed, while the Ga3d peak now clearly can be seen. However, as more cleaning cycles are employed, there are no further drastic changes in the spectrum. Since the Ga4d peak does not become narrower, there is a possibility of GaO still remaining on the surface, thus rendering the 2-step cleaning process only partially successful.
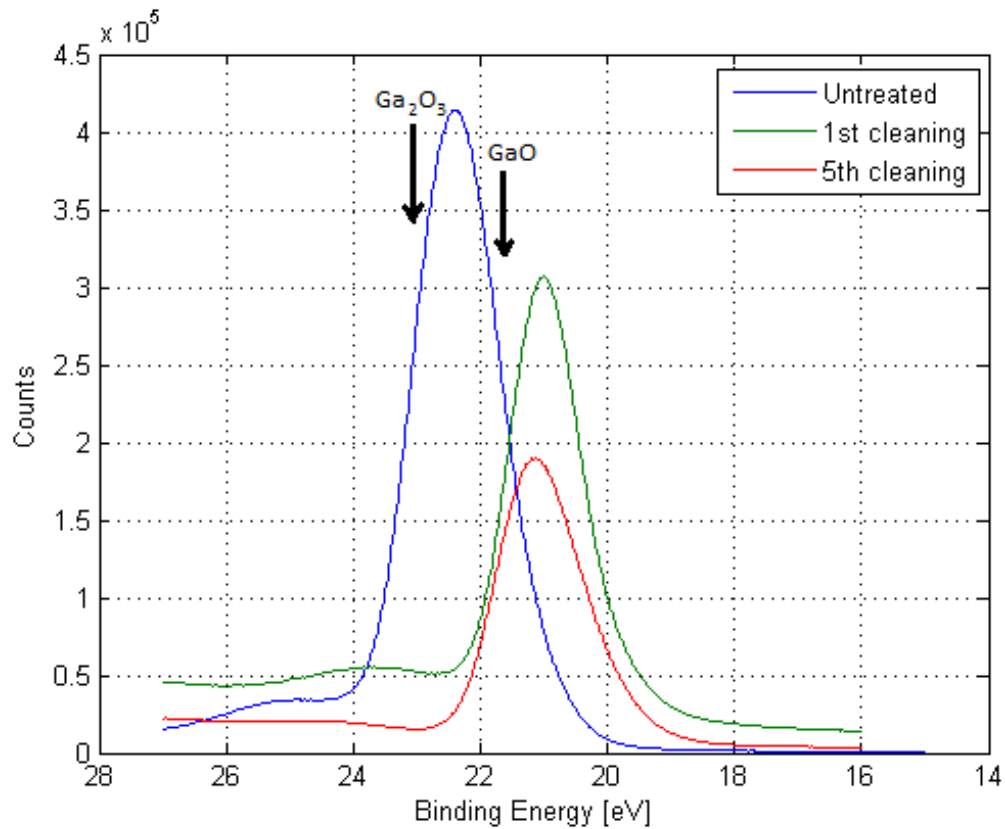

Figure 32: Merged diagram showing the emergence of the Ga3d peak.

There are also several factors which should be taken into account when evaluating XPS data, although hard to compensate for. From the various images, it is clear that there is a general broadening of the peaks and sometimes no well defined energy can be established. The reasons for this might include, amongst other things, finite life time of the electrons in an excited state, phonons invoked in the sample by e.g. temperature fluctuations and instrumental broadening caused by the photon beam having an ever so slight energy distribution [34].

5.4 Nanowires

When yearning for the construction of devices made out of nanowires, it is generally impossible to pick specific wires as one pleases. A blind-pick from a collection of nanowires should preferably always result in a clean wire. It is therefore required that after an applied cleaning recipe, an acceptable number of randomly studied wires should show clean and ordered facets.

However, several problems arise when scanning on surfaces haphazardly covered with nanostructures such as nanowires. The first and perhaps the most obvious issue is to actually locate a wire. Given a diameter of 80 nm that is hopefully aligned perpendicular to the movement of the piezoelectric element, the process can at times be very time consuming even though their general area can be identified using a powerful CCD camera. Further, a very high loop in conjunction with a slow scan speed gain must be used in order not to crash the tip into the nanowire once located, as they are huge compared to variations in the substrate. This is aptly illustrated in fig. 34(a). Note that no hexagonal structure can be observed while scanning using these parameters, as the tip retracts heavily while approaching a wire.

The nanowires endured a total of three cleaning cycles, totalling 80 minutes at 395° C, twice at a chamber pressure of $2 \cdot 10^{-6}$ mbar and once at $2 \cdot 10^{-5}$ mbar. Once on top of a nanowire, the loop gain and scan speed can be returned to usual values. A resulting image can be seen in fig. 33, scanned at a sample bias of $V_g = -2.5$ V and a tunnelling current of $I_t = 120$ pA. Along the length of the wire, several lines of lumps can be seen stretching across its width. These might originate from various sources, although the most probable is remnant oxides sticking to stacking faults in the facet from when the wire was grown.
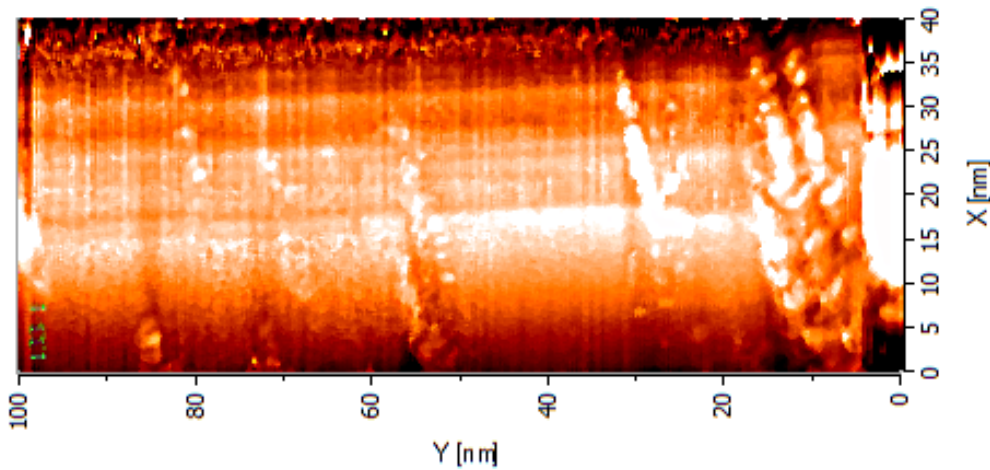

Figure 33: STM image of a 40×100 nm^2 InAs nanowire.

Once a sufficiently flat area on a nanowire has been located, it can be probed closer, all while making sure not to fall off the edge during scanning. The rows in fig. 34(b) can all clearly be seen to run perpendicular to the growth direction, which is an indication of the $\{10\bar{1}0\}$ facet as shown in fig. 5. The distance between two adjacent lines was averaged to 0.647 nm, Even though segments of the nanowires appear completely clean, there are still oxides present as can be seen towards the top of the image, preventing further atomic resolution.
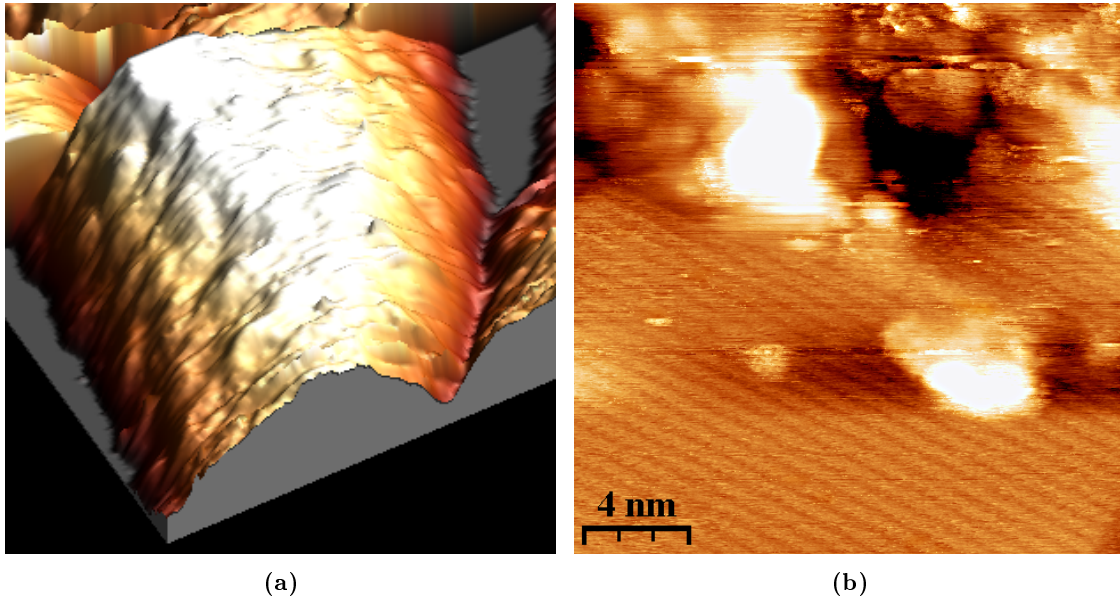

(a)   (b)

Figure 34: STM images of InAs nanowires. (a) 3D representation of a nanowire with a diameter of 80 nm. The narrowing towards the lower part of the image might indicate the base or tip of the wire. (b) Close-to atomic resolution on top of the flat, hexagonal WZ structure.
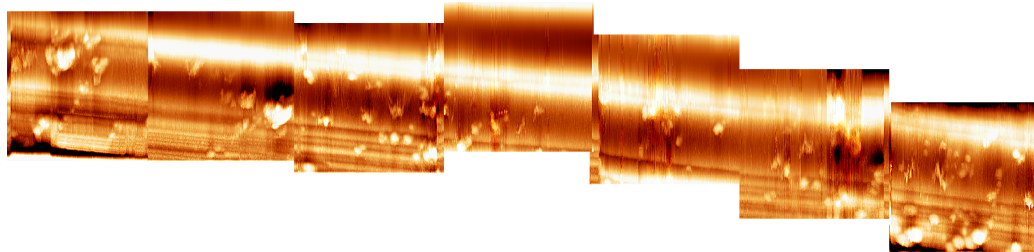

Figure 35: Bonus image of a segmented nanowire consisting of several STM scans along the same wire.

6 Conclusion and Outlook

In summary, several different materials have been examined throughout this thesis, with primary focus on the III-V semiconducting compounds. These were studied with either directly or indirectly two Nobel prize awards; namely the STM and XPS. The former yielded down-to atomic scale imagery of the sample surfaces while the latter provided detailed information regarding the elements present on the samples. The materials studied include wafers of Au, GaSb, as well as both wafers and nanowires consisting of InAs.

Generally, it was found that successful cleaning of said materials can be done by exposing them to a flux of atomic hydrogen along with some moderate annealing. The Au wafers were studied in order to evaluate the quality of the in-house constructed Tungsten tips before performing any measurements on the remaining samples.

Three different crystal planes of InAs were studied: (111)A, (111)B and (110). Proper atomic resolution was only achieved for the (110) plane, although clean surfaces for each could be attained showing the overall morphology of the surfaces, allowing for some conclusions to be made. The (111)A plane was found to exhibit a rectangular $(2{\times}2)$ reconstruction of the surface, while the (111)B plane was believed to be unreconstructed. Regarding the two InAs(110) samples that were studied, one was ruined due to a contamination of tungsten while the other allowed for accurate measurements of material properties such as its lattice constant, which also correlated well with previously determined values.

Two different crystal planes of GaSb were studied: (100) and (110), and both proved very hard to clean successfully. However, small seemingly clean patches of the (100) surface were attained but only at high annealing temperatures. This clean patch managed to shed some faint light on the surface morphology, as measurements hinted of a (1×2) reconstruction of the surface.

The error estimates provided during the measurement of material-specific properties such as their lattice constant were merely chosen with respect to the min/max deviation between the peaks, as they were not entirely well-defined. As previously mentioned, any measurement with the current resolution will at best be a rough approximation, as the same area might even express slightly different features between a scan upwards and downwards. The reader should instead remind themselves that we are dealing with atomic scale measurements, probing *individual atoms* given the right circumstances. Even the smallest disturbance might thus result in catastrophic consequences.

Generally regarding all STM measurements, there were a few error estimates to keep it mind. Firstly, it is literally impossible to keep track of a single area throughout different cleaning cycles to see how it changes, unless cleaned *during* the actual scanning which was not possible with the STM system used during the present work. Secondly, every measurement required a sample bias much higher than the actual band gap of the material, which implies less-than-optimal conditions.

XPS data of GaSb(100) suggested that desorption of oxides does indeed occur even at lower temperatures, although not completely, as traces of GaO was believed to remain on the surface. This might explain why no clean surfaces could ever be imaged during STM measurements, as only the very top surface layer is probed. Further, the interpretation regarding which peaks remained and which disappeared was up for debate, as especially oxides sticking to every other element present on the sample are hard to keep track of.

Unfortunately, nanowires were only properly studied towards the very end of the assigned time for this work. Hence, not much data was successfully obtained other than, much like their wafer counterparts, they could successfully be cleaned using the current methods; it is merely a task of tweaking the parameters. A series of electrical measurements were indeed performed on the very same batch of wires, comparing the outputs before and after cleaning with atomic hydrogen. Alas, even if esaki diode behavior emerged only *after* being cleaned, it was not meant to be a part of this thesis.

Given more time, it would have been desirable to properly figure out a cleaning cycle which worked for GaSb(100) at lower temperatures, since there appears to be a demand of constructing various devices out of nanowires consisting of both InAs and GaSb. Additionally, further STM measurements performed after high-temperature cleaning of GaSb(100) and/or LEED measurements are needed in order to confirm or dismiss the suggested (1×2) reconstruction of the surface, as the author currently has no other data or sources to back up this claim. GaSb has only been studied a fraction as much as the III-V giants GaAs and InAs, and generally accepted theories regarding e.g. surface structures are sparse.

7 Bibliography

References

[1] P. Hofmann, *Solid State Physics: An Introduction*, Wiley-VCH, 2008

[2] CNRS (Délégation Paris Michel-Ange), 25 April, 2012. What is the best way of stacking apples? *ScienceDaily*. Retrieved 02 June, 2013, from http://www.sciencedaily.com/releases/2012/04/120425094304.htm

[3] R. F. C. Farrow, *Molecular Beam Epitaxy - Applications to Key Materials*, William Andrew Publishing/Noyes, 1995.

[4] M. Hjort, *Direct imaging and electrical probing of nanowire surfaces*, Lund University, 2008.

[5] G. Binnig and H. Rohrer, *IBM Journal of Research and Development*, 1986, **30**, 4.

[6] G. Binnig and H. Rohrer, *Reviews of Modern Physics*, 1987, **59** (3), 615-625.

[7] G. Binnig and H. Rohrer, *Surface Science*, 1986, **126**, 236-244.

[8] R. J. Hamers, *The Journal of Physical Chemistry*, 1996, **100** (31), 13103-13120.

[9] J. Knutsson, *Morphological Studies of Nanowire Surfaces Using Scanning Probe Techniques*, Master's thesis, Lund University, 18 June, 2012.

[10] G. Binnig and H. Rohrer, *Ultramicroscopy*, 1983, **11**, 157-160.

[11] Mehmet Z. Baykara and Omur E. Dagdeviren and Todd C. Schwendemann and Harry Mönig and Eric I. Altman and Udo D. Schwarz, *Beilstein Journal of Nanotechnology*, 2012, **3**, 637-650.

[12] H. Heinrich, *Annalen der Physik*, 1887, **8**, 983-1000.

[13] *University of Alabama*, Retrieved 22 May, 2013, from bama.ua.edu/ surfspec/cha_details.htm

[14] *MaxLab*. Retrieved 04 June, 2013, from https://www.maxlab.lu.se/node/1597

[15] Gh. Tahmasebipour, Y. Hojjat, V. Ahmadi and A. Abdullah, *International Journal of Advanced Manufacturing*, 2009, **44**, 80-90.

[16] I. Ekvall, E. Wahlström, D. Claesson, H. Olin and E. Olsson, *Measurement Science and Technology*, 1999, **10**, 11-18.

[17] V. Repain, J. M. Berroir, S. Rousset and J. Lecoeur, *Europhysics Letters*, 1999, **47** (4), 435-441.

[18] *Wafer Technology Ltd.* Retrieved 20 May, 2013,
from http://www.wafertech.co.uk/

[19] *Dr. Eberl MBE-Komponenten GmbH.* Retrieved 25 May, 2013, from http://www.mbe-komponenten.de/products/mbe-components/gas-sources/habs.php

[20] T. D. Veal and C. F. McConville, *Applied Physics Letters*, 2000, **77**, 1665-1667.

[21] G. R. Bell, N. S. Kaijaks, R. J. Dixon and C. F. McConville, *Surface Science*, 1998, **401** (2), 125-137.

[22] G. R. Bell and C. F. McConville, *Applied Physics Letters*, 1996, **69** (18), 2695-2697.

[23] *SVT Associates, Inc.* Retrieved 25 May, 2013,
from http://www.svta.com/rf-plasma-sources.html

[24] I. Horcas, R. Fernandez, J.M. Gomez-Rodriguez, J. Colchero, J. Gomez-Herrero and A. M. Baro, *Review of Scientific Instruments*, 2007, **78**, 013705.

[25] A. Depuydt, N.S. Maslova, V.I. Panov ,V.V.Rakov, S.V. Savinov and C. Van Haesendonck, *Applied Physics A*, 1998, **66**,

[26] X. Lopez-Lozano, C. Noguez and L. Meza-Montes, *Revista Mexicana de Física*, 2005, **51** (2), 168-175.

[27] A. Taguchi and K. Kanisawa, *Applied Surface Science*, 2006, **252** (15), 5263-5266.

[28] E. Hilner, E. Lundgren and A. Mikkelsen, *Surface Science*, 2010, **604**, 354-360.

[29] G. R. Bell and C. F. McConville, *Applied Physics Letters*, 1996, **69** (18), 2695-2697.

[30] H. Kroemer, *Physica E*, 2004, **20**, 196-203.

[31] D. K. Biegelsen, R. D. Bringans, J. E. Northrup and L. -E. Swartz, *Physical Review B*, 1990, **41** (9), 5701-5706.

[32] T.D. Veal, M.J. Lowe, C.F. McConville, *Surface Science*, 2002, **499**, 251-260.

[33] *X-Ray Data Booklet: Section 1.1 ELECTRON BINDING ENERGIES*, Retrieved 16 June, 2013 from http://xdb.lbl.gov/Section1/Sec_1-1.html

[34] N. Vinogradov, *Controlling Electronic and Geometrical Structure of Honeycomb-Lattice Materials Supported on Metal Substrates*, PhD thesis, Uppsala University, 5 April, 2013.